Coherent Anti-Stokes Raman Spectroscopy (CARS)

Mazza, Francesco; Castellanos, Leonardo; Kliukin, Dmitrii; Bohlin, Alexis

DOI
10.1007/978-981-97-1703-3_13

Publication date
2024

Document Version
Final published version

Published in
Springer Series in Optical Sciences

Chapter 13
Coherent Anti-Stokes Raman Spectroscopy (CARS)

Francesco Mazza, Leonardo Castellanos, Dmitrii Kliukin, and Alexis Bohlin

13.1 Introduction

Optical diagnostics are the main experimental tools for the quantitative measurements in chemically reacting flows, with unparalleled performance in terms of precision and accuracy, spatio-temporal resolution, and response time [1, 2]. The use of various forms of light-matter interaction to extract information on the velocity field, chemical composition and local thermodynamic properties allows for in situ measurements to be performed in harsh measurement conditions that physical probes could not withstand. Secondly, while the introduction of physical probes inevitably alters the flow-field we set out to measure [3], optical diagnostics can realize truly non-perturbative measurements. The coherent nature of the light provided by laser sources can be used to focus the light with lenses which translates into an excellent spatial resolution unachievable with alternative measurement techniques. Furthermore, the availability of pulsed laser sources with repetition rates in the kHz range or faster results in the "freeze of the flow field" with high sampling rates that are thus capable of measuring highly dynamic and transients phenomena in reacting flows [2]. In view of this, many specialized laser-based techniques have been developed to measure key physical and chemical properties in gas-phase reacting flows. Chief among these is laser spectroscopy, which allows for quantitative measurements of important scalar quantities in harsh environments such as flames, plasmas and high-speed/high-enthalpy flows [4, 5]. Raman spectroscopy in particular provides non-perturbative, in situ thermometry in high-temperature flames, as well as concentration measurements of major

F. Mazza · L. Castellanos · D. Kliukin · A. Bohlin (✉)
Department of Aerospace Engineering, Delft University of Technology, Kluyverweg 1, 2629 HS Delft, The Netherlands
e-mail: alexis.bohlin@gknaerospace.com

A. Bohlin
Space Campus, Luleå University of Technology, Bengt Hultqvists Väg 1, 98128 Kiruna, Sweden

Inspection Technologies, GKN Aerospace Engine Systems, Trollhättan, Sweden

D. K. Singh et al. (eds.), *Raman Spectroscopy*, Springer Series in Optical Sciences 248,
https://doi.org/10.1007/978-981-97-1703-3_13

species, and Raman-based techniques are the most commonly employed for scalar determination in combustion environments [1].

Raman scattering is nevertheless a rather inefficient optical process, the typical Raman cross-section being in the order of 10^{-29} cm^2/molecule/steradian in gas-phase media [6]. In addition, spontaneous Raman scattering is an incoherent process, leading to the isotropic emission of the signal: single-shot Raman spectroscopy thus requires large collection optics and suffer from the often presence of luminous background due to e.g. flame chemiluminescence or fluorescence in plasma reactors. The intensity of the scattered radiation can be enhanced by several orders of magnitude if the molecules can be made to re-emit the incident light coherently. In coherent anti-Stokes Raman spectroscopy (CARS) we implement this idea by employing additional input laser fields to excite the Raman modes to be probed in the scattering process. The resulting CARS signal is spatially and temporally coherent, such that it can be detected remotely from the measurement location and easily be discriminated from the incoherent background in luminous harsh environments.

The potential of CARS for scalar determination in gas-phase media [7, 8] was realized soon after the first observation of this phenomenon by Maker and Terhune [9], and continuous efforts over the last five decades have made this technique into the gold standard for gas-phase thermometry and concentration measurements [10]. In this context, two diverging trends can be identified in the development of gas-phase CARS diagnostics. The first is the strive for diagnostics completeness, developing new diagnostics schemes to extend the number of scalar fields observed simultaneously on the basis of a single-shot measurement. This kind of research efforts lead to e.g. multiplex CARS for the simultaneous interrogation of multiple Raman-active species [11, 12], and to the extension of CARS to measure velocity, as well as density and pressure [13, 14]. On the other hand, the relevant use of CARS as a diagnostic tool for industrial applications pushed the technique in the opposite direction, aiming to the development of portable, field-deployable systems, capable of robust operations in practical measurement scenarios [15–17].

The present chapters describes some of the most recent advancements in gas-phase CARS with particular focus on two-beam femtosecond/picosecond (fs/ps) CARS [18] and its development in terms of correlated imaging measurements and wideband multiplex detection capabilities on the one hand, and simplified system architecture on the other. This recent progress establishes two-beam fs/ps CARS as the state-of-the-art for multi-fields scalar measurements in chemically reacting flows and provide a convincing pathway for the prospect use in a wide range of industrial applications, with unparalleled measurements fidelity and spatio-temporal resolution.

13.2 Fundamentals of Coherent Anti-Stokes Raman Scattering

Contrary to linear spontaneous Raman scattering, CARS is a third-order non-linear optical process, consisting of the four-wave mixing (FWM) of three input laser fields—called the "pump" (oscillating at optical frequency ω_{pump}), the "Stokes" (ω_{Stokes}), and the "probe" (ω_{probe})—to produce the CARS polarization field [19]:

$$P_{\text{CARS}}^{(3)} = \frac{3i\omega_{\text{CARS}}}{2nc}\chi_{\text{CARS}}^{(3)}E_{\text{pump}}E_{\text{Stokes}}^{*}E_{\text{probe}} \tag{13.1}$$

where ω_{CARS} is the frequency of the CARS signal, $\chi_{\text{CARS}}^{(3)}$ is the third-order non-linear optical susceptibility of the optical medium, l is the interaction length, and nc is the speed of light in the medium.

As illustrated in Fig. 13.1, the frequency of the CARS field is dictated by the conservation of energy in the light-matter interaction, such that:

$$\omega_{\text{pump}} - \omega_{\text{Stokes}} + \omega_{\text{probe}} - \omega_{\text{CARS}} = 0 \tag{13.2}$$

where the negative sign in front of the Stokes and CARS frequency indicate that these field are emitted from the medium as a result of, respectively, stimulated and spontaneous Raman scattering of the incident pump and Stokes fields.

Two different kind of CARS processes are illustrated in Fig. 13.1a, b: respectively, a ro-vibrationally resonant and a non-resonant (NR) CARS process. The former is realized when the frequency difference between the pump and Stokes fields is resonant to a rotational-vibrational mode of the optical medium, such that the Raman mode is coherently excited. The establishment of rotational-vibrational coherent in the molecular medium results in the coherent scattering of the incident probe field, such that the scattered radiation is spatially coherent. The propagation direction of the CARS signal satisfies the so-called "phase matching" for the non-linear optical process, conserving linear momentum in the process:

$$\Delta\boldsymbol{k} = \boldsymbol{k}_{\text{pump}} - \boldsymbol{k}_{\text{Stokes}} + \boldsymbol{k}_{\text{probe}} - \boldsymbol{k}_{\text{CARS}} = 0 \tag{13.3}$$

where $\boldsymbol{\Delta k}$ is the phase mismatch, and $\boldsymbol{k}_i$ is the wave vector of the ith field involved in the FWM process. The phase matching of the CARS process in a non-collinear BOXCARS [20] geometry is sketched in Fig. 13.1c.

The resonant CARS process is subject to the same selection rules that apply to spontaneous Raman scattering. In the simplest case of CARS on simple homonuclear diatomic molecules such as N_2, the selection rules for pure-rotational and ro-vibrational CARS are respectively:

$$\begin{aligned} \Delta v &= 0 \\ \Delta J &= \pm 2 \end{aligned} \tag{13.4}$$

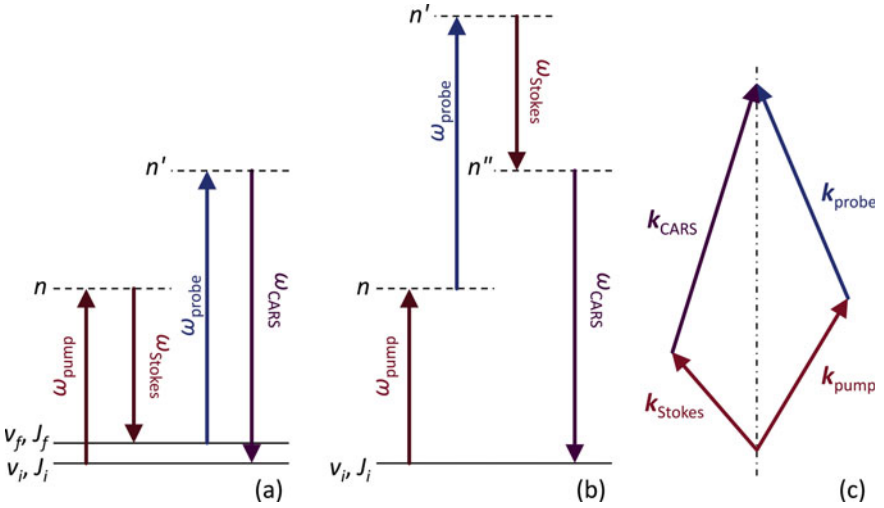

Fig. 13.1 Energy and momentum conservation in the CARS process. Energy diagram for the resonant **a** and non-resonant. **b** CARS processes. In the former, the frequency difference between the pump and Stokes fields is resonant to the molecular transition between the initial (v_i, J_i) and final rotational-vibrational (v_f, J_f) energy states. n, n', n'': virtual electronic states. **c** Phase-matching of the CARS process. The planar BOXCARS phase-marching sketched here allows for a perfectly phase-matched CARS process (i.e. $\Delta \boldsymbol{k} = \boldsymbol{0}$) with crossed-beam geometry

and

$$\begin{aligned} \Delta v &= 1 \\ \Delta J &= 0, \pm 2 \end{aligned} \tag{13.5}$$

where v is the vibrational quantum number and J is the total angular momentum (or rotational) quantum number, and the spectral branches corresponding to the rotational selection rules $\Delta J = -2, 0, 2$ are indicated according to the usual notation as O-, Q- and S-branch, respectively [21]. Through the third-order non-linear optical susceptibility in (13.1) the CARS signal carries information about the statistical population distribution of the Raman-active molecules over their rotational and vibrational energy manifolds. For a thermalized gas-phase medium, this corresponds to the rotational and vibrational Boltzmann distribution: CARS can thus be employed to perform high-fidelity thermometry in gas-phase media.

The NR CARS process in Fig. 13.1b does not involve any rotational or vibrational resonance in the optical medium: upon the interaction with the pump, Stokes and probe fields, the interacting molecule is found in a "virtual" electronic state, for which an instantaneous dephasing can be assumed. The spectrum of the NR CARS signal is then a continuum which carries no information on the internal energy distribution of the scatterers. Nevertheless, this signal plays an important role in the CARS experimental routine, as we will discuss in the following.

13.2.1 Frequency-Resolved CARS

Since its first demonstration in gas-phase media [8], CARS has been developed in the most powerful laser diagnostics to measure temperature and major species concentrations in combustion environments [4]. Of all the many research efforts spent in the development of gas-phase CARS: of particular relevance to the content of present chapter is the development of dual-broadband CARS, first introduced by Eckbreth and Anderson for multi-species spectroscopy [11], and subsequently demonstrated in Aldén et al. for pure-rotational CARS spectroscopy [12].

The main idea behind pure-rotational dual-broadband CARS is illustrated in Fig. 13.2a: by employing broadband pump and Stokes pulses, the whole manifold of pure-rotational modes can be simultaneously excited, allowing for the single-shot detection of all the different rotationally Raman-active species present in the probe volume. Since the first demonstration by Aldén and co-workers, pure-rotational dual-broadband has been vastly employed in combustion diagnostics, both in laboratory flames [22, 23] and in industry-relevant applications [24, 25].

The use of nanosecond (ns) laser sources, typically Nd:YAG lasers, provides high spectral resolution in CARS measurements, allowing for resolving e.g. closely-spaced rotational lines in the ro-vibrational spectrum of N_2 [26], or assigning the spectral lines due to different species in the pure-rotational Raman spectrum [27]. Nevertheless, there are a number of factors that ultimately limit the accuracy and precision of ns CARS techniques. The most significant is certainly the impact of molecular collisions, which determine the dephasing of the rotational-vibrational Raman coherence on a timescale of typically some hundreds ps in atmospheric gas-phase media. The ns pulses employed to realize frequency-domain CARS are much longer than that, hence the collisional Raman linewidths are paramount to accurate CARS measurements [28]. As the collisional environment is typically unknown—the concentration of major collisional species being indeed an objective of CARS measurements–, molecular collisions represent a significant source of uncertainty for ns CARS. Similarly the interference with NR CARS signal, whose intensity depends on the local composition of the optical medium in the probe volume, adds to the uncertainty in the evaluation of the CARS spectra especially at high pressure [24]. Furthermore, the multi-mode broadband dye lasers employed to realize multiplex CARS are affected by mode noise [29], which limits the inherent single-shot precision of CARS thermometry to ~3%.

These limitations have pushed further the development of novel experimental approaches to gas-phase CARS diagnostics, leading to the introduction of time-resolved CARS techniques, which solve most of the major limitations of ns CARS.

13.2.2 Time-Resolved CARS

The development of time-resolved CARS techniques has been propelled by the recent commercial availability of regenerative fs laser amplifiers, providing mJ-level energies with pulse duration <100 fs.

Employing short fs laser pulses, the rotational-vibrational coherence of the target molecules can be impulsively excited and maximized, thus enhancing the intensity of the CARS signal significantly [30]. As seen in Fig. 13.2, the molecular coherence, as encoded in the third-order non-linear optical susceptibility $\chi^{(3)}_{\mathrm{CARS}}$ in (13.1), shows quantum revivals with a period of some ps for the simple diatomic molecules investigated by gas-phase CARS. Hence, the use of ultrashort (ps or fs) probe pulses results in high temporal resolution, such that the evolution of the Raman coherence can be measured in a time-resolved fashion. The main dephasing mechanism for the Raman coherence in gas-phase atmospheric media is due to molecular collisions: time-resolved CARS measurements can be performed below the typical collisional timescale (~100 ps), resulting in near collision-independent measurements [31]. The benefit is two-fold: on the one hand, this reduces the measurement uncertainty due to the unknown collisional environment [32] and, on the other, the collisional Raman linewidths can be directly measured by the time-resolved dephasing of the CARS signal [33, 34]. Furthermore, the high peak power of fs laser pulses, combined with the most efficient impulsive excitation of the Raman coherence, allows for extending the CARS capability beyond point measurements to realize imaging spectroscopy [18, 35–37], as we will detail in the following section.

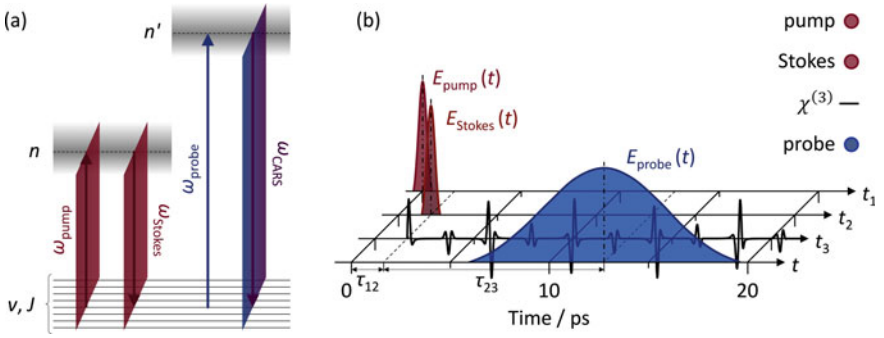

Fig. 13.2 Dual-broadband pure-rotational CARS. **a** Energy diagram for the dual-broadband CARS process. By employing broadband pump and Stokes pulses multiple Raman modes can be simultaneously excited: the excitation bandwidth corresponds to the spectral cross-correlation of the two pulses $E_{\mathrm{pump}}(\omega) \star E_{\mathrm{Stokes}}(\omega)$. **b** Schematic of the hybrid fs/ps CARS process in the time-domain. The combined interaction of the fs pump and Stokes laser pulses excites the non-linear optical response $\chi^{(3)}$ of the gas-phase medium (N_2 is simulated here), which evolves in time through quantum revivals. The longer ps probe pulse "reads" multiple revival peaks, which enhance the encoding of the underlying Raman modes in the frequency-resolved CARS spectrum

A detailed overview of the many time-resolved CARS techniques developed over the past two decades is beyond the scope of the present chapter, and the reader is referred to the specialized literature (see e.g. [2, 10]). In the following, referencing is only made to hybrid fs/ps CARS, which combines broadband fs and relatively narrowband ps laser pulses to perform simultaneously time- and frequency-resolved measurements [38]. As shown in Fig. 13.2b, fs pump and Stokes pulses are used to impulsively excite the Raman coherence in the gas-phase medium, while a ps laser pulse serves as the probe, providing sufficient spectral resolution for analyzing the CARS spectrum. The possibility of delaying the probe pulse with respect to the fs pump and Stokes pulses furthermore allows for time-gating the generation of the NR CARS background. Due to the instantaneous dephasing of the electronic coherence in the virtual states of Fig. 13.1b, this signal is only generated when the pump, Stokes and probe fields are temporally overlapped. In the past ten years, hybrid fs/ps CARS has become established as the state-of-the-art for scalar measurements in gas-phase media, allowing for high-fidelity, in situ thermometry and species concentration measurements in combustion [2, 39] and plasma environments [40, 41].

13.3 Two-Beam fs/ps CARS Instrument

One of the most significant advancements in hybrid fs/ps CARS for gas-phase diagnostics was the development of two-beam fs/ps CARS. This technique is based on a novel phase-matching scheme introduced by Bohlin and Kliewer [18], and first demonstrated by the authors by performing pure-rotational fs/ps CARS over a one-dimensional field-of-view (FOV). Figure 13.3 illustrates the principle of two-beam fs/ps CARS in the time- and frequency-domain. Contrary to the conventional implementation of hybrid fs/ps CARS—which employs two fs laser pulses at distinct carrier frequencies to provide the pump and Stokes fields and excite the target Raman modes–, the two-beam phase-matching scheme makes use of a single broadband fs pump/Stokes laser pulses to excite the Raman coherence. As a laser pulse with duration <100 fs has a large bandwidth spanning some tens of nm (for a carrier wavelength of 800 nm), constructive pump/Stokes frequency pairs can be found across the entire bandwidth of a single fs laser pulse. For example a 45 fs laser pulse, as employed in [18], thus has sufficient bandwidth to effectively excite Raman modes in the pure-rotational region of the spectrum up to ~500 cm^{-1}.

This allows for a great simplification of the hybrid fs/ps CARS instrument as a single regenerative fs laser amplifier provides the laser pulse needed to excite the pure-rotational coherence of most species of interest in gas-phase media. The authors reported significantly improved signal levels, owing to the pulse energy available to the pump and Stokes fields provided by the single fs laser pulse, and to the ease of alignment of the two laser beams. The inherent spatial and temporal overlap of the pump and Stokes fields guaranteed by this two-beam scheme was furthermore proposed to improve the robustness of hybrid fs/ps CARS against beam steering in turbulent measurement environments.

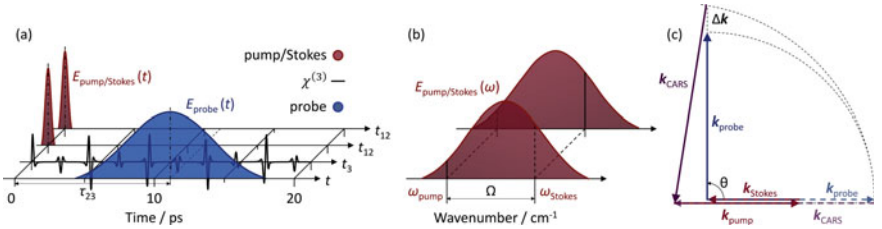

Fig. 13.3 The two-beam CARS phase-matching scheme. **a** Schematic of two-beam fs/ps CARS in the time domain. $E_{\text{pump/Stokes}}(t)$, and $E_{\text{probe}}(t)$ represent the temporal envelops of the combined pump/Stokes and probe pulses, respectively. $\chi^{(3)}$ is the nonlinear optical susceptibility of the gas-phase medium due to the coherent motion of its molecular components. t_{12} and t_3 are the coherence timescales during the interaction with the input laser pulses, while τ_{23} is the intra-pulse delay. **b** Spectral excitation in two-beam fs/ps CARS. Constructive pump/Stokes frequency-pairs at Raman shifts $\Omega = |\omega_{\text{pump}} - \omega_{\text{Stokes}}|$ are found across the bandwidth of a single broadband fs excitation pulse. Since the pulse has finite bandwidth, the excitation efficiency decreases monotonically with increasing Raman shift. **c** Phase-matching of two-beam fs/ps CARS. The two-beam fs/ps CARS process sketched here can only be perfectly phase-matched (i.e. $\Delta\boldsymbol{k} = 0$) if all the laser beams are collinear. Adopting a crossed-beam geometry (i.e. $\theta \neq 0°$, with crossing angle θ), necessarily results in a phase-mismatch that increases with larger Raman shifts and crossing angle [18]

A significant advantage of the two-beam scheme over alternative phase-matching geometries, such as BOXCARS [20] and collinear single-beam CARS [42], is the high spatial resolution available and its straightforward tuneability, achieved by adjusting the incident crossing angle between the pump/Stokes and probe beams. Bohlin and Kliewer demonstrated a longitudinal resolution of their two-beam fs/ps CARS instrument, as dictated by the interaction length between the two laser beams, of ~50 μm for a crossing angle of 90°, an improvement of almost two orders of magnitude with respect of typical BOXCARS configurations [36]. It should be noted nonetheless that the improvement in the spatial resolution comes at the expense of a perfect phase-matching geometry, introducing a phase-mismatch that grows with the crossing angle and Raman shift, ultimately limiting the efficiency of the CARS signal generation for high-energy Raman modes.

The most consequential development of gas-phase CARS introduced with the two-beam phase-matching scheme, is undoubtedly the possibility of performing coherent imaging spectroscopy over linear and planar FOVs. Employing cylindrical focusing optics to form the laser beams into sheets, crossed over a ~6 mm line at the measurement location, and coherent imaging optics to perform spatial imaging spectroscopy, the authors demonstrated the possibility of retrieving spatially-correlated spectral information over this 1D FOV with an ~60 μm line-spread function (LSF). Following work from the same research group demonstrated the use of this technique to investigate the flame-wall interaction in a head-on quenching (HOQ) burner, resolving the temperature gradient evolution through the impingement of the CH_4/air flame onto a metal wall of the HOQ burner and its subsequent quenching [43]. More recently, Escofet-Martin and co-authors have employed a similar two-beam fs/ps

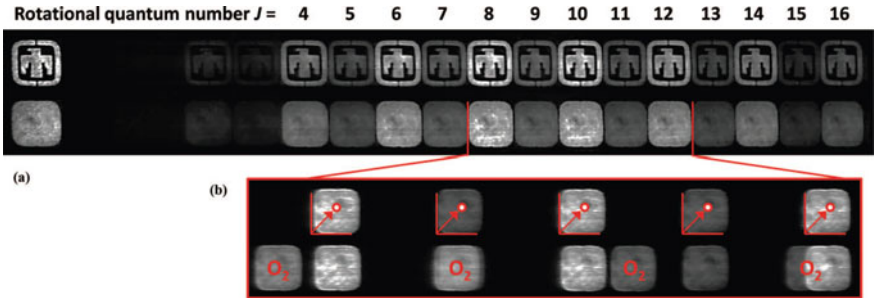

Fig. 13.4 Two-beam fs/ps planar CARS imaging (2D-CARS). **a** Single-shot hyperspectral N_2 CARS image recorded at room temperature. In the first row, a mask is placed on the probe beam path to illustrate the imaging quality of the CARS instrument. **b** High-spectral resolution 2D CARS images acquired in N_2 (first row) and O_2 (second row), each square image corresponding to an isolated line in the pure-rotational Raman spectrum. Each image consists of ~125 × 120 pixels, corresponding to ~15000 spatially correlated spectra recorded with a single-shot. Adapted with permission from Bohlin and Kliewer [37]. © 2013 AIP Publishing LLC

CARS instrument to study the transient heat transfer in the boundary layer at the flame-wall interface [44].

Furthermore, this two-beam fs/ps CARS phase matching scheme was later extended to perform hyperspectral imaging, as shown in Fig. 13.4. Crossing the pump/Stokes pulse laser formed into a laser sheet with an unfocused collimated probe beam, Bohlin and Kliewer showed that the CARS signal can be generated and recorded over the resulting ~2 × 20 mm planar FOV, thus realizing for the first time 2D CARS in gas-phase media [37]. The great diagnostic potential of this 2D CARS instrument was then demonstrated by the same authors, by simultaneously mapping the temperature and species concentration fields over planar slices in a laminar premixed CH_4/air flame [45] and in a turbulent H_2 jet flame [46].

13.3.1 State-of-the-Art Capabilities

As a continuation on these works we have recently introduced several advancements to the pure-rotational two-beam fs/ps CARS technique. For example, the possibility of employing a single ultrafast regenerative amplifier laser system to build a two-beam fs/ps CARS instrument with single-shot 1D imaging capabilities at temperatures higher than 2000 K was first demonstrated in Castellanos et al. [47]. This system employs an ultrafast regenerative amplifier system (7.5 mJ, 1 kHz, Astrella Coherent) as the single laser source to generate both the broadband fs pump/Stokes pulse and the relatively narrowband probe pulse, as shown in Fig. 13.5. The laser amplifier provides two repetition-wise synchronized output beams. The first one is a 4.5 mJ compressed near transform-limited (TL) 35 fs duration laser pulse centered at a wavelength of 800 nm, which undergoes second-harmonic bandwidth compression

(SHBC, Light Conversion) to generate a narrowband probe pulse. In the SHBC unit the 35 fs TL pulse is equally split in two pulses, to which a conjugate linear chirp is applied before recombining them in a $\chi^{(2)}$ non-linear crystal [48]. The sum-frequency generation (SFG) of the phase-conjugated chirped pulses results in an ~4 ps probe pulse centered at 400 nm, obtained with a ~30% conversion efficiency. Third-order chirp terms arising in the SHBC result in the detrimental presence of spectral sidebands in the spectrum of the ps probe pulse [49], which are here suppressed by introducing a tunable pulse shaper, consisting of two high-resolution transmission gratings (3039 lines/mm, >90% transmission efficiency, Ibsen Photonics), two cylindrical lenses with a 300 mm focal length, and a mechanical slit, all mounted in a 4f arrangement. By tuning the slit aperture in the Fourier plane of the pulse shaper, the probe duration can be tuned in the range ~5–15 ps, with a corresponding pulse energy of 1.2–0.3 mJ. The second, uncompressed, output of the ultrafast regenerative amplifier is sent to an external grating compressor to generate the 35 fs TL pump/Stokes pulse: the use of an external compressor unit allows for a flexible compensation (pre-chirping) of dispersion terms along the optical path, maximizing the excitation bandwidth at the measurement location. The linear polarization states of the pump/Stokes and probe pulses are independently controlled by half-wave plates for 800 nm and 400 nm, respectively. An optical delay line controls the relative arrival of the pump/Stokes and probe pulses at the measurement location.

The same two-beam phase matching geometry of [18] is adopted with cylindrical lenses (CL_h, f: = 500 and 300 mm, respectively) forming the pump/Stokes and probe beams into two laser sheets, and is crossed with an incident angle of ~3°. The FOV is set to ~1.3 mm by employing an astigmatic focusing configuration, with cylindrical

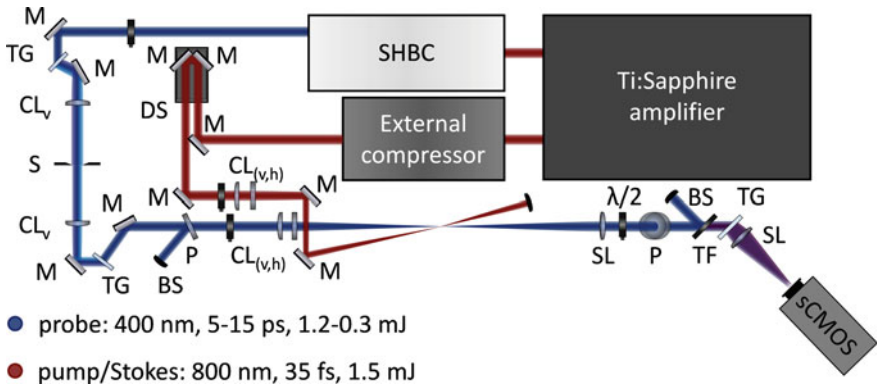

Fig. 13.5 Schematic drawing of the two-beam fs/ps 1D-CARS imaging instrument developed in [47]. A single Ti:sapphire ultrafast regenerative amplifier system is employed to generate the 35 fs pump/Stokes and the ~5–15 ps probe pulses. Cylindrical lenses, mounted in an astigmatic focusing configuration, form the laser beams into two sheets at the measurement location, where they cross to form a ~1.3 mm measurement line. TG, transmission grating; S, slit; CL, cylindrical lens with vertical (v) and horizontal (h) symmetry axes; λ/2, half-wave plate; B, burner; P, polarizer; SL, spherical lens; M, mirror

lenses with vertical symmetry axes (CL_v, f: = 1000 and 300 mm) in combination with horizontal axes compressing the height of the pump/Stokes and probe laser sheets. The CARS signal is collected in a wide-field slit-less coherent imaging spectrometer and imaged 1:1 onto a sCMOS detector (Zyla, Andor), allowing for 200 × 2048 pixel image acquisition at 1 kHz frame rate, thus matching the repetition rate of the laser system. This is the first use of a sCMOS camera in the context of gas-phase fs/ps CARS proving that—despite the limited depth of the quantum well, as compared to conventionally employed back-illuminated water-cooled CCD devices—such detectors can be effectively employed to perform CARS imaging at high repetition rates in combustion environments. The combination of high-resolution transmission grating and 400 mm imaging lens allows for spectral images to be recorded over the whole pure-rotational region of the Raman spectrum 0–525 cm^{-1}, with spectral resolution of 0.25 cm^{-1}/pixel, allowing for the simultaneous detection of major combustion species (for example: N_2, O_2 and H_2).

The 1D-CARS system capability as a powerful combustion diagnostics tool is thus demonstrated by performing simultaneous thermometry and relative O_2/N_2 concentration measurements across a laminar premixed CH_4/air flame front, as shown in Fig. 13.6. The gradients in the two scalar fields are simultaneously resolved along the 1D FOV and tracked in time with a repetition rate of 1 kHz, much faster than the 13 Hz oscillations induced by buoyancy effects in the flame, and well-resolved in the temporal traces of Fig. 13.6. These flame measurements furthermore provide a benchmark for the performance of the CARS instrument in terms of thermometric precision and accuracy, which are estimated to be 0.7% and 2.5% respectively, at a temperature of ~1700 K.

As compared to previous implementations of two-beam fs/ps CARS imaging instruments, such as in [18, 43, 44], the use of a single laser source to provide both the fs pump/Stokes and the ps probe pulses guarantees the inherent synchronization of the pulses at the measurement location, with no temporal jitter. Moreover, the use of a 400 nm probe, as generated by the SHBC from the 800 nm fs pulses, when compared to conventional external ps lasers with a carrier wavelength of 532 nm [18, 43, 44], is beneficial in terms of signal generation and spatial resolution. The intensity of the CARS signal scales with the squared frequency of the signal itself, such that reducing the probe wavelength from 532 to 400 nm results in a gain in the signal intensity by a factor ~2. In addition, employing a shorter wavelength improves the focusing properties of the probe pulse and the diffraction-limited resolution of the imaging optics in the CARS spectrometer. In [47] the line-spread function of the imaging spectrometer is measured to be ~20 μm, a significant improvement over the best reported value of ~40 μm in [50]. The temperature and O_2 concentration gradients in Fig. 13.6 are thus smoothly sampled by ~25 independent measurement points. Its superior spatial resolution makes this CARS imaging instrument ideal for the detailed investigation of the physics of premixed H_2 flame propagation, which is characterized by a steep temperature gradient whose spatial undersampling can give a large measurement uncertainty.

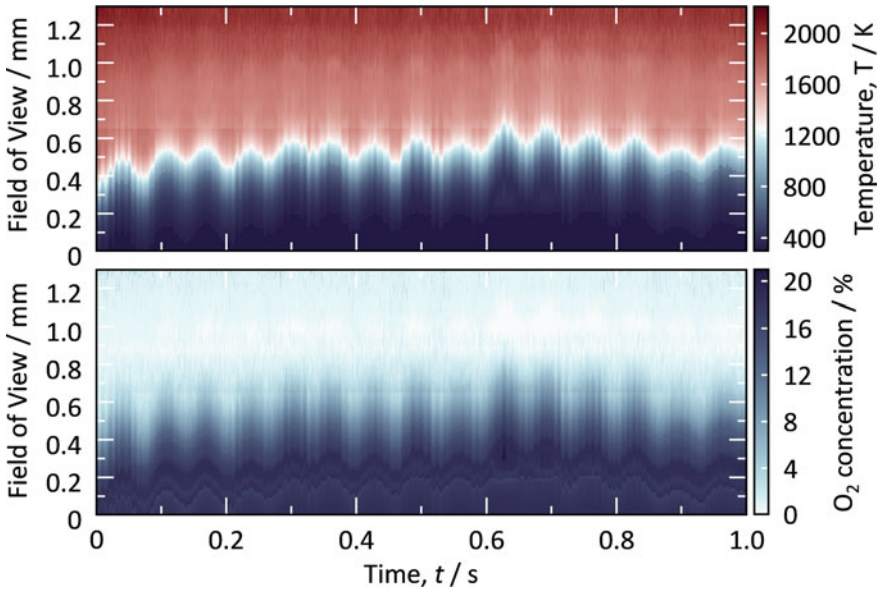

Fig. 13.6 Simultaneous thermometry and relative O_2/N_2 concentration measurements by two-beam fs/ps 1D-CARS imaging across a laminar premixed CH_4/air flame front. **a** Temperature gradient across the flame front mapped by single-shot fs/ps 1D-CARS at 1 kHz. The inflection point in the temperature profile ($T \approx 1200$ K at this flame condition) is used to define the location of the flame front at each single-shot spectral image. **b** Relative O_2/N_2 concentration measured by pure-rotational fs/ps CARS across the laminar flame front. As expected the O_2 concentration gradients is inversely correlated to the local temperature profile

Finally, the space-time correlated resolution obtained with the CARS imaging measurements allows for deconvolving fluctuations in the experimental flame platform, due e.g. to buoyancy forces (as observed in Fig. 13.6), Helmholtz resonances in the burner, or fluctuation in the mass flow-controllers. Apart from the importance on deducing the flame physics more accurately, the capability in space-time correlated resolution is also beneficial at the assessment of the performance of the fs/ps CARS instrument itself. If the uncertainty in the boundary conditions is not mapped properly, the presence of large fluctuations built-in at the benchmarking experimental platform can largely shadow the inherent stochastic error, which is solely dependent of the laser diagnostic instrument. Barros and co-workers, for example, have recently reported a thermometric precision better than 0.5% in a laminar premixed CH_4/air flame when removing the dynamic contribution due to flame oscillations [51]. In [47] as well as in Mazza et al. [52], analogous flame oscillations are resolved in the temporal evolution of the temperature gradient, measured over the 1D FOV. This space-time correlated resolution thus allows for defining the flame front location at each single-shot spectral image—identified as the position of the inflection point in the temperature gradient–, and tracking its oscillations as shown in Fig. 13.7. Since these oscillations are only mechanical in nature, the measurement statistics

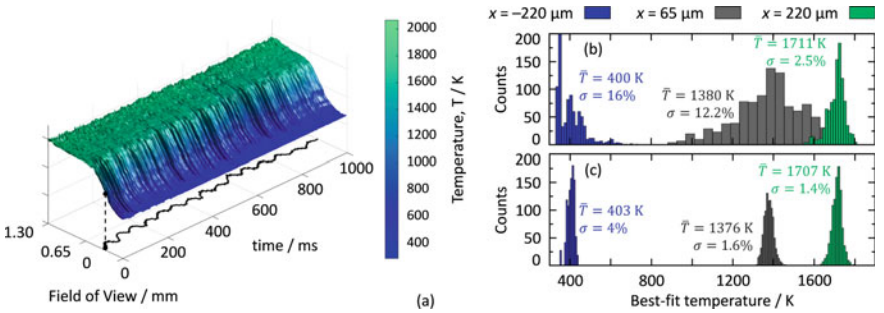

Fig. 13.7 Conditional mapping of the flame front by fs/ps 1D-CARS imaging. **a** Temperature gradient across the laminar premixed CH_4/air flame front, as mapped by single-shot fs/ps 1D-CARS imaging over the ~1.3 mm FOV performed at 1 kHz. The location of the flame front is subject to low-frequency oscillations at ~13 Hz, which affect the evaluation of the single-shot precision of the CARS instrument. **b** Histogram of the temperature measured by pure-rotational fs/ps CARS at three distinct locations along the flame front. In the reactants (blue) 220 µm before the temperature inflection point ($x = 0$ mm); inside the reaction layer (gray) at $x = 65$ µm; and in the combustion products (green) at $x = 220$ µm after the temperature inflection point. **c** Histogram of the temperature measured at three locations conditional to the position of the flame front in each single-shot spectral image. The conditional mapping of the flame front position removes the measurement uncertainty arising from the physical oscillations in the flame platform. The inherent single-shot precision of the fs/ps CARS instrument can thus be assessed

can thus be collected conditional to the distance from the flame front, rather than at a fixed point over the FOV. Figure 13.7 illustrates the substantial improvement in the resulting standard deviation of the temperature statistics measured over 1000 single-shot spectra at three locations in the flame. Upon deconvolving the physical fluctuations of the flame platform used to benchmark the fs/ps CARS instrument, the thermometric precision is consistently found to be ~0.7% in [47, 52].

13.3.2 Limitations

The complex chemistry often encountered in chemically reacting flows in industrial applications pose rather demanding requirements on the fidelity of the experimental data available to validate predictive engineering models. Temperature, in particular, is the key scalar controlling the chemical reaction rates and thus determining the chemical pathways for the reactions. An instructive example of this being the impact of the flame temperature on the formation of NO_x in methane combustion at the pressure and temperature found in a typical aircraft turbo-engines (inlet conditions: 30 atm, 900 K). A measurement uncertainty of ~1% in the measured temperature results in a change of ~20% in the amount of thermal NO_x predicted by Arrhenius-type reaction rates [53]. The high spectral stability of presently commercially-available fs laser systems, and the development of time-resolved CARS techniques –minimizing the impact of the unknown collisional environment on the CARS spectra, and the

relating experimental uncertainty, even at pressures as high as 70 bar! [49]—presently make hybrid fs/ps CARS the gold standard for spatially resolved thermometry. The single-shot precision and the accuracy of hybrid fs/ps CARS at flame temperature are estimated to be ~1–2% and ~2–3%, respectively [50, 54, 55]. Furthermore, the possibility of employing a single ultrafast regenerative amplifier system to generate all the laser pulses has recently pushed the precision of hybrid fs/ps CARS thermometry consistently below the 1% limit [47, 51, 52, 54, 56].

An outstanding source of uncertainty in two-beam fs/ps CARS measurements is the excitation efficiency of the various Raman modes within the bandwidth of the fs pump/Stokes pulse [57–59]. As a single broadband fs laser pulse is employed to impulsively excite the rotational Raman coherence, the number of constructive pump/Stokes frequency pairs available to excite a specific Raman mode is determined by the spectral autocorrelation of the fs pulse itself. This can be measured by the spectrum of the NR CARS signal generated in a medium with no active Raman modes, e.g. in Argon (Ar). As no rotational-vibrational coherence is generated in the medium, the NR CARS signal is instantaneously dephased and its spectrum is a continuum profile that maps the spectral excitation efficiency. The conventional fs/ps CARS experimental routine thus entails the measurement of the NR CARS spectrum, to subdivide the resonant CARS spectra (spectral referencing) as shown in Fig. 13.8, such that quantitative information about the local temperature and composition of the gas-phase medium can be retrieved. The NR CARS signal is then measured ex situ in a non-resonant Ar, sequentially to the CARS experiment. The effective excitation efficiency profile available at the measurement location (in situ) can nonetheless be affected by the shot-to-shot stability of the laser source employed [29, 57, 60, 61], as well as by the propagation of the laser pulses to the measurement location.

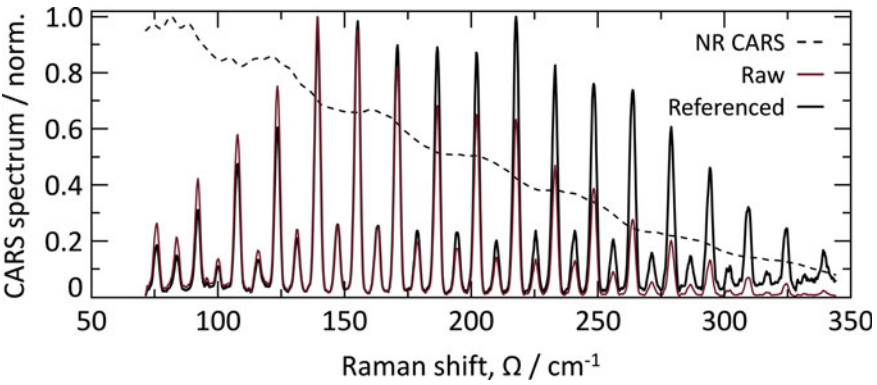

Fig. 13.8 Spectral referencing for pure-rotational CARS. The single-shot pure-rotational N_2 CARS spectrum (solid red line), acquired in a laminar premixed CH_4/air flame, is subdivided by the NR CARS spectrum acquired ex situ in room-temperature Ar (dashed line). The solid black line is the resulting referenced spectrum that can meaningfully be compared to the rotational Boltzmann population distribution of the N_2 molecules

Different schemes have been demonstrated for the concurrent ex situ generation of the NR CARS signal top monitor the shot-to-shot fluctuations in the spectral excitation efficiency [16, 58, 59]. Nevertheless, these cannot account for the temporal chirp introduced to short fs pump/Stokes pulses as they propagate through different optical materials towards the measurement location. Hence, the impact of the spectral referencing protocol on the accuracy of fs/ps CARS thermometry is still largely unexplored.

Besides there is an increasing interest in the development of fs/ps CARS to realize complementary spectroscopy, by simultaneously investigating the pure-rotational and ro-vibrational regions of the Raman spectrum [62]. In the context of gas phase diagnostics, there are several motivations to extend the applicability of two-beam fs/ps CARS beyond the pure-rotational region:

- Some molecules that play a major role in combustion environments and other chemically reacting flows are difficult to detect and quantify by means of pure-rotational CARS. For example, major combustion products or pollutant species (e.g. H_2O [63] and CO [64]) have extremely low rotational Raman cross-sections, such that they give rise to weak CARS signals in high temperature environments. The example of water vapor is rather illustrative: H_2O is a major product of combustion processes and CARS techniques have been applied to its ro-vibrational (ν_1 mode) spectrum since the 1980s to measure temperature and concentrations in flames [65–68]. On the other hand, the application of pure-rotational CARS to water vapor lead Nordström and co-workers to the conclusion that it would not be possible to use this technique to measure temperature and H_2O concentrations in combustion environments [63]. Even worse is the case of CH_4, a spherical-top polyatomic molecule with no rotational degree of freedom in its ground vibrational state, and thus rotational Raman-inactive.
- The H_2 molecule is rotationally Raman-active however, since it is light weight, has a relatively low moment of inertia spinning around its centro-symmetric axis, and has an uncommonly large rotational constant ($B \approx 60.8$ cm^{-1} [69]), such that its pure-rotational spectrum spans more than 1500 cm^{-1} at flame temperature [70]. The application of fs/ps CARS to investigate the H_2 spectrum in the pure-rotational region is thus limited to the first two spectral lines at 354 and 587 cm^{-1}, as shown in Fig. 13.9. While these are typically sufficient to measure the relative H_2/N_2 concentration at low temperature [71, 72], the shift in the rotational Boltzmann population distribution with the increasing temperature ultimately limits the detection of H_2 by pure-rotational fs/ps CARS [73].
- Alongside its use in combustion diagnostics, gas-phase CARS has found vast application to perform thermometry in harsh plasma environments. The use of laser spectroscopy in this context is particularly useful as it can provide complementary information on the vibrational and rotational Boltzmann population distributions where significant thermal non-equilibrium conditions exist (e.g. dielectric-barrier discharges [74] and arc discharges [75]). The ability of simultaneously performing pure-rotational and ro-vibrational spectroscopy on the same Raman-active molecule, e.g. by dual-broadband dual-pump fs/ps CARS as in

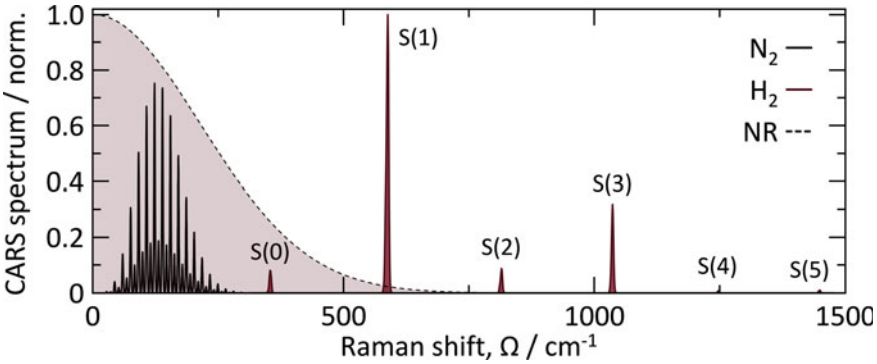

Fig. 13.9 Pure-rotational two-beam fs/ps CARS for simultaneous thermometry and relative H_2/N_2 concentration measurements. The simulated excitation profile provided by a 35 fs TL pump/Stokes pulse is represented by the shaded red area: only the first two lines in the pure-rotational Raman spectrum of H_2 can be coherently excited by the spectral breadth of this pump/Stokes pulse

[40] makes fs/ps CARS the ideal tool to investigate rotational-vibrational non-equilibrium. On these grounds ultrabroadband CARS has been developed, which employs supercontinuum laser pulses—with bandwidth of many tens or hundreds of nm—to simultaneously excite the rotational and vibrational coherence of the Raman-active molecules over a large portion of the Raman spectrum. A first example of this approach is found in Tedder et al., who employed a broadband ns dye laser (∼18 nm FWHM) to perform dual-pump CARS, simultaneously probing N_2, O_2, H_2, C_2H_4, CO and CO_2 in the spectral region ~1000–2500 cm^{-1} [76].

13.4 Polarization-Sensitive CARS Imaging Spectrometer

The measurement uncertainty introduced by the spectral referencing protocol in pure-rotational fs/ps CARS thermometry is addressed in Mazza et al. by introducing a novel experimental protocol for the concurrent in situ generation of the NR CARS signal [52]. This protocol is implemented by a polarization approach [62, 77], whereby the linear polarization states of the pump/Stokes and probe pulses is determined such that the resonant and NR CARS signal are cross-polarized. Introducing a polarization gate in the wide-field coherent imaging spectrometer is thus possible to discriminate the two signal components and record them simultaneously in distinct detection channels.

To this effect, a novel polarization-sensitive coherent imaging spectrometer is developed in [52], as illustrated in Fig. 13.10. Half-wave plates for 800 and 400 mm control the linear polarization of the pump/Stokes and probe pulses respectively, and the relative polarization angle between the two is set to be $\tan^{-1}\sqrt{6} \approx 67.8°$. This "magical" angle is demonstrated to generated the NR CARS signal with linear polarization orthogonal to that of the resonant CARS signal for completely depolarized

Raman transitions, as is the case for pure-rotational spectra [73]. The two signal components are nearly co-propagating with the probe beam, for the two-beam phase matching geometry and shallow crossing angle employed. These are collimated by a 400 mm spherical lens and their polarization is rotated by a 400 nm half-wave plate, to align it to the P- and S-polarization direction of a thin-film polarizer. After the half-wave plate the resonant signal is P-polarized with respect to and transmitted through the polarizer, while the NR signal is reflected by it and collected in a second detection channel. The latter consists of a mirror and a second 400 nm half-wave plate, which turns the polarization of the NR signal by 90°: the signal components have the same polarization, such that the diffraction efficiency of the transmission grating (Ibsen Photonics) is >90% in both detection channels. An angle-tunable band-pass filter (bandwidth FWHM: 20 at 400 nm, Semrock) suppresses the probe beam before the transmission grating. Both CARS signals are imaged 1:1 onto two 200 × 2048 pixels regions of the sCMOS detector by the 400 mm spherical lens, so that high-resolution CARS spectra can be acquired in the pure-rotational region up to ~500 cm^{-1}. This spectrometer design allows for multidimensional fs/ps CARS, as the spatio-temporal and spectral resolutions are complemented by the sensitivity to the linear polarization angle of the CARS signal. An innovative design combining the polarization-sensitive dual-channel configuration with 2D hyperspectral imaging capabilities is further proposed in [78]: this extends the CARS measurement capability over 5 dimensions (x–y in space, in spectrum, in time, and in polarization), while avoiding the convolution of space and frequency for relatively broadband spectral features.

The use of the coherent imaging spectrometer to address the measurement uncertainty inherent to the spectral referencing protocol [52] is addressed in the next paragraph. In Kliukin et al. the polarization sensitivity of the spectrometer is exploited to

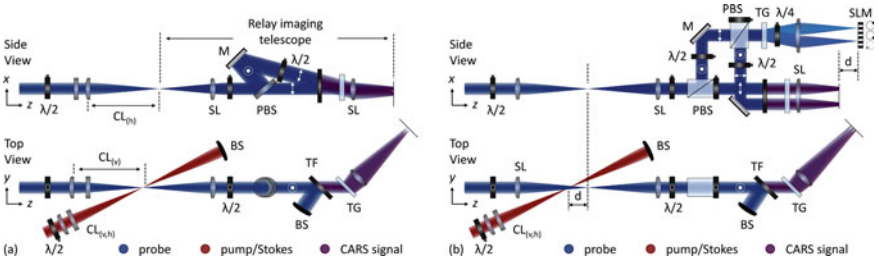

Fig. 13.10 Schematic of the polarization-sensitive coherent imaging spectrometer. Two separate detection channels for P- and S-polarized light, with orientation determined with respect to the polarization beam splitter (PBS), are relay-imaged onto the sCMOS sensor. **a** 1D CARS imaging configuration with astigmatic cylindrical focusing of the pump/Stokes and probe beams. Adapted with permission from Mazza et al. [52]. © 2020 Elsevier Inc. **b** 2D hyperspectral imaging. A 4f pulse shaper, consisting of transmission grating (TG), spherical lens (SL) and spatial light modulator (SLM), allows for the application of the in situ referencing protocol to the 2D CARS spectral images. Adapted with permission from Kliukin and Bohlin [78] M, mirror; λ/2 half-wave plate; λ/4, quarter-wave plate; BS, beam stop; TF, tunable band-pass filter; CL, cylindrical lens

investigate the origin of a high-order cascaded CARS (CCARS) signal and proposed as a novel diagnostic tool to measure local fluctuations in the flow composition with unparalleled sensitivity [79]. This work is illustrated in Sect. 13.4.2. Finally, the polarization approach developed for the discrimination of the resonant and NR CARS signals can be extended to realize dual-probe fs/ps CARS [80–82] and measure the effect of the collisional environment on the pure-rotational Raman coherence. As discussed in Sect. 13.4.3 this approach can be employed to determine the concentration of water vapor in H_2/air flames [72], which cannot be attained by conventional frequency-resolved CARS in the pure-rotational region.

13.4.1 In Situ Referencing of the Spectral Excitation Efficiency

The polarization-sensitive coherent imaging spectrometer described in the previous paragraph is employed in Mazza et al. to perform coherent Raman imaging thermometry with in situ referencing of the spectral excitation efficiency [52]. The resonant and NR CARS signals are simultaneously generated over the 1D FOV placed orthogonally across a laminar premixed CH_4/air flame front, as shown in Fig. 13.11.

The gradient in the temperature and O_2 concentration along the reaction layer of the flame is evidently manifested in the resonant CARS image detected in

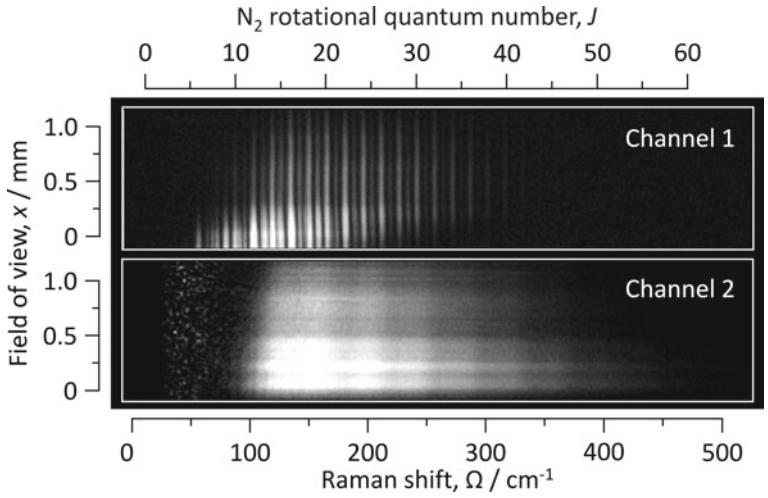

Fig. 13.11 Single-shot fs/ps CARS imaging in the pure-rotational region of the Raman spectrum, with simultaneous detection of the resonant and NR CARS signals. The measurements are performed across a laminar premixed CH4/air flame front ($\phi = 0.95$). The resonant CARS signal is detected "Channel 1" and correspond to the pure-rotational CARS spectrum of N_2 and O_2. The broadband NR CARS signal is detected in "Channel 2". Adapted with permission from Mazza et al. [52]. © 2020 Elsevier Inc.

"Channel 1". In the lower portion of the FOV (i.e. from $x = 0$ mm) the cold reactants are probed and the pure-rotational CARS spectra present the spectral signatures of N_2 and O_2, the main component of ambient air. In addition, only lower rotational energy states are thermally populated at room temperature according to Boltzmann statistics. Moving inside the thin chemical reaction layer of the flame front, O_2 is consumed in the combustion reaction and the heat released by it increases the local temperature, as measured by the pure-rotational Raman spectrum on N_2, which spreads to higher rotational energy states. The temperature change is also evident in the reducing intensity of the NR CARS signal along FOV in "Channel 2", in agreement with the quadratic scaling of the CARS signal intensity with the number density of the gas-phase medium. Each NR spectrum along the FOV of Fig. 13.11 maps the excitation efficiency of the pure-rotational Raman modes in the corresponding resonant CARS spectrum at the same location along the measurement line.

In order to understand the impact of the spectral referencing protocol on the accuracy of pure-rotational fs/ps CARS thermometry, the NR CARS spectra recorded in situ simultaneously to the flame spectra are compared to the NR spectra acquired sequentially in a room-temperature Ar flow (ex situ) in Fig. 13.12. The difference between the two spectral referencing protocol is clarified by comparing the NR CARS spectra measured ex situ and in situ at two different locations along the 1D FOV of the fs/ps CARS instrument. At $x = 0.4$ mm, corresponding to the average location of the temperature inflection point in the flame front measurements, the two average NR CARS spectra perfectly coincide. Adopting either the ex situ or in situ referencing protocols results in the same normalization of the resonant CARS spectra: the conventional ex situ referencing protocol does not introduce any systematic bias in pure-rotational fs/ps CARS thermometry at this location. The situation is quite different when considering the NR CARS spectrum generated in the hot product gases of the flame at location $x = 1$ mm, and comparing it to the NR CARS spectrum measured in Ar at the same location. The effective excitation efficiency available at this measurement location, as mapped by the in situ NR CARS spectrum, is larger than assessed by the NR spectrum measured ex situ. The conventional experimental protocol is thus predicted to introduce a systematic overestimation of the local temperature at this measurement location in the flame.

The mismatch between the spectral excitation efficiency profiles measured ex- and in situ is explained in [52] by the fs pump/Stokes pulse propagation to the measurement location and the impact of the temporal chirp imparted by different optical materials on the effective spectral excitation efficiency. In particular, the temperature gradient across the FOV entails a corresponding gradient in the effective refractive index of the optical medium. Hence, different portions of the pump/Stokes beams experience a different group velocity dispersion (GVD) while propagating through the flame to the measurement location. The relatively cold gas-phase medium in the reactants and pre-heat zone of the flame introduces a larger GVD than the rarefied hot product gases, resulting in the observed variation of the spectral excitation efficiency over the FOV of the fs/ps CARS instrument. The conventional ex situ referencing protocol is unable to account for the effect of the local temperature and composition on the fs pump/Stokes pulse propagation, and thus introduce a systematic bias in

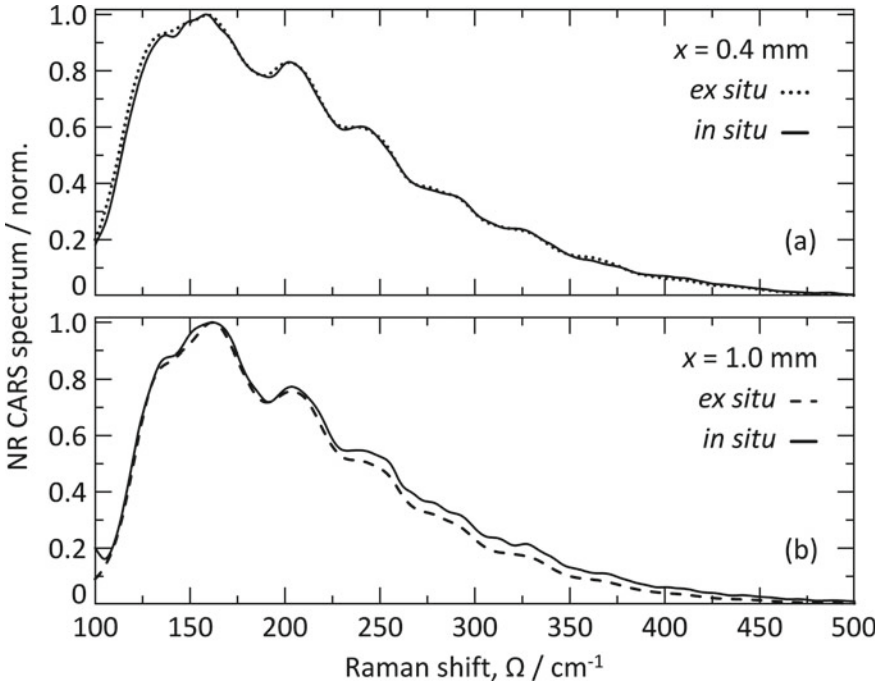

Fig. 13.12 Ex situ and in situ referencing for 1D pure-rotational fs/ps CARS imaging. **a** Comparison between the ex- (dotted line) and in situ (solid line) spectral excitation efficiency profiles at $x = 0.4$ mm. **b** Comparison of the excitation profiles measured ex- (dashed line) and in situ (solid line) in the products of the flame at location $x = 1$ mm

the fs/ps CARS thermometry. This is estimated in the flame experiment of [52] to amount to ~1.3% of the evaluated temperature.

These results show how the spectral referencing protocol can introduce an additional uncertainty in pure-rotational fs/ps CARS thermometry, which is most relevant when short fs laser pulses (<50 fs) are employed to impulsively excite the rotational Raman coherence. This uncertainty should be taken into account when pursuing exact CARS diagnostics, to cope with the demanding fidelity requirements for experimental measurements in chemically reacting flows. The novel experimental protocol for the in situ referencing of the spectral excitation efficiency is thus proposed to further advance state-of-the-art pure-rotational fs/ps CARS, pushing the measurement uncertainty (both stochastic and systematic) consistently below the "dream-limit" of 1%.

13.4.2 CCARS

The large peak power offered by fs laser pulses not only allows for the efficient excitation of the Raman coherence and the possibility of extending the measurement capability to fs/ps CARS imaging, but can also results in higher-order non-linear optical effects accompanying the CARS process [83].

One such higher-order process is the cascading effect of the CARS signal depicted in Fig. 13.13. When the amplitude of the CARS field is sufficiently high, it can be significantly scattered by the Raman-active molecules, effectively acting as a probe field in a second-order coherent scattering process. This cascading effect can proceed to higher orders, as reported e.g. by Liu et al., who observed CCARS up to the 58th order in gaseous CO_2 [84]. As the spectrum of the CARS signal in Fig. 13.13d is discrete in nature—each spectral line corresponding to a pure-rotational Raman transition of N_2–, the resulting CCARS spectrum is the superposition of the pure-rotational Raman spectra originated by its individual lines. This explains the ~4:3 intensity ratio for even and odd lines in the CCARS spectrum, while the well-known 4:1 ratio in the CARS spectrum is explained by the nuclear spin multiplicity of the N_2 molecule. Furthermore, the pure-rotational O- and S-branch CCARS spectra are shifted by $6B$ (with rotational constant $B \approx 2$ cm^{-1} for N_2) on both sides of each spectral line of the CARS spectrum. As a result, the CCARS lines appear exactly between the lines of the CARS spectrum and are well resolved by the coherent imaging spectrometer discussed above. The theory developed to describe the polarization dependence of the CARS signal on the polarization states of the pump/Stokes and probe pulses can be easily extended to describe the CCARS signal, as sketched in Fig. 13.13d. By employing a relative polarization angle of 70.5° between the pump/Stokes and probe pulses, the CARS and CCARS signals are cross-polarized and can be independently recorded in the two detection channels of the polarization-sensitive coherent imaging spectrometer.

The simultaneous single-shot detection of the CARS and CCARS signals in gas-phase media offers a unique opportunity to develop a highly non-linear optical diagnostic tool with unparalleled sensitivity to local changes in species concentrations. This is because of the CCARS process being a $\chi^{(5)}$ non-linear optical process, characterized by the following scaling law:

$$I_{\mathrm{CCARS}} \propto \left|\chi^{(3)}_{\mathrm{CARS}}\right|^4 \left(\frac{\omega_{\mathrm{CARS}}\omega_{\mathrm{CCARS}}}{c^2}\right)^2 l^4 I^4_{\mathrm{pump/Stokes}} I_{\mathrm{probe}} \tag{13.6}$$

where $I_{\mathrm{pump/Stokes}}$ and I_{probe} are the intensities of the pump/Stokes and probe laser pulses, and ω_{CCARS} is the frequency of the CCARS field. Through the third-order non-linear optical susceptibility of the optical medium $\chi^{(3)}_{\mathrm{CARS}}$ the CCARS signal scales with the fourth power of the number density of molecular scatterers, $I_{\mathrm{CCARS}} \sim \mathrm{N}^4$. This scaling relationship is verified in [79] by varying the relative concentration of N_2 in binary mixture with Ar from 30 to 80%. The CARS and CCARS signal are simultaneously recorded in the two detection channels of the polarization-sensitive

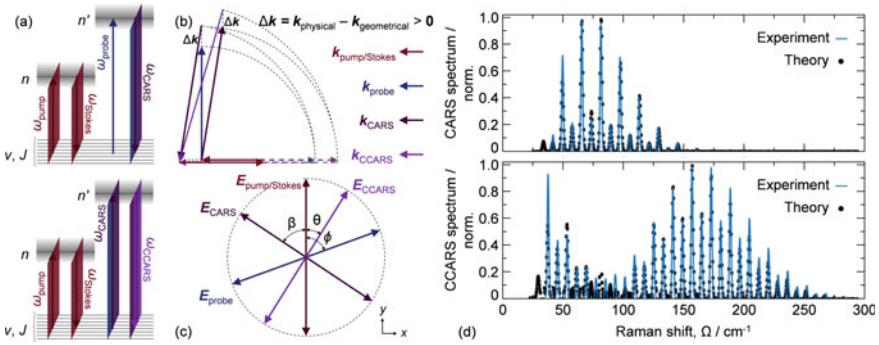

Fig. 13.13 Cascaded fs/ps CARS. **a** Energy diagram of two-beam pure-rotational fs/ps CARS and CCARS. **b** Two-beam quasi phase-matching diagram for the CARS and CCARS processes with (i) all-collinear beams and (ii) 90° crossing angle between the pump/Stokes and probe beams. The CCARS signal is generated by the CARS field acting as a probe beam. **c** Polarization settings to generate the CARS and CCARS signals with orthogonal polarization states. **d** Single-shot fs/ps CARS (top) and CCARS (bottom) spectra recorded in room-temperature N_2. Adapted with permission from Kliukin et al. [79]. © 2021 John Wiley & Sons Ltd.

coherent imaging spectrometer and subdivided to measure the absolute concentration of N_2 molecules in the probed volume, according to $I_{\mathrm{CCARS}}/I_{\mathrm{CARS}} \sim N^2$.

The simultaneous detection of the CARS and CCARS signals can thus be employed as a calibration-free diagnostic for absolute concentration and density measurements. In particular, owing to exponential-order higher sensitivity of the CCARS signal to the number density of the molecular scatterers, this technique could find application in the quantification of local fluctuations in bulk mixture composition, due e.g. to differential diffusion effects. A prospect application is the measurement of the H_2 transport in turbulent flows, where the large mass diffusivity of the lightweight H_2 molecule is known to play a significant role, and experimental data are much needed for the validation of numerical models [85].

13.4.3 CARS Probing the Invisible!

The low rotational Raman cross-section of the H_2O molecule and the complexity of its pure-rotational Raman spectrum [63] present a formidable obstacle to the detection and quantification of water vapor in high-temperature environments via pure-rotational fs/ps CARS. On the other hand, water vapor is one of the major products of the combustion reaction, and the only one such in the case of H_2/air flames: its quantification is thus critical to be able to monitor the progress of the chemical reaction in situ. While a pure-rotational CARS signal generated by the water molecules in these environments, this is effectively "invisible" to the fs/ps CARS instrument, as it is largely overshadowed by the orders-of-magnitude stronger pure-rotational CARS signal from N_2 molecules [63].

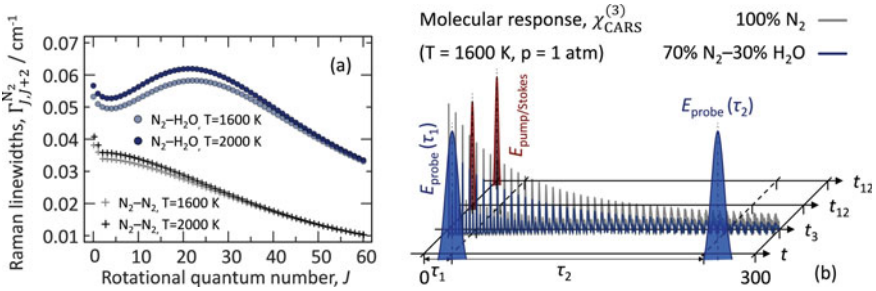

Fig. 13.14 Detection scheme for water vapor via time-resolved measurements of the collisional dephasing of the pure-rotational Raman coherence of N_2. **a** Collisional Raman linewidths for N_2 (radiator) perturbed by N_2 and H_2O collisional partners at combustion-relevant temperatures. **b** Dual-probe time-resolved fs/ps CARS measurements of the collisional dephasing of the pure-rotational Raman coherence of the N_2 molecules

Castellanos et al. present an alternative approach to the measurement of water vapor concentrations in H_2 flames by the time-resolved collisional dephasing of the pure-rotational N_2 CARS signal [72]. While the signature of the H_2O molecules can hardly be detected in the pure-rotational Raman spectrum, these play a significant impact on the evolution of the pure-rotational coherence of the more easily-detected N_2 molecules. Under atmospheric pressure conditions, the evolution of the rotational coherence of a thermal ensemble of N_2 molecules is determined by inelastic collisions between the coherently-rotating N_2 molecules (radiators) and other collisional partners (perturbers) [86]. The rotational energy transfer (RET) determined by inelastic collisions is thus responsible for the dephasing for the dephasing of the pure-rotational CARS signal. The RET rates, quantified by the collisional Raman linewidths $\Gamma^{N_2}_{J,J+2}$, depend on: (i) the rotational state of the radiator, (ii) the temperature of the gas-phase medium, and (iii) the nature of the perturber molecules as seen in Fig. 13.14. In particular, H_2O perturbers are responsible for a larger dephasing of the N_2 CARS signal than N_2 perturbers and the N_2-H_2O Raman linewidths present a largely non-monotonic dependence on the rotational quantum number J [87].

In H_2/air flames, water vapor is the only major species that cannot be directly detected in the frequency domain, while N_2, O_2 and H_2 all present strong signatures in the pure-rotational region of the Raman spectrum. Temperature, density and relative O_2/N_2 and H_2/N_2 concentrations can be simultaneously measured by use of the pure-rotational fs/ps CARS instrument described in the previous section. Hence, the collisional environment and resulting dephasing of the pure-rotational N_2 CARS signal can be specified up to one unknown: the H_2O concentration. The diagnostic strategy presented in [72] exploits the simultaneous spectral and temporal resolution of this pure-rotational fs/ps CARS instrument to measure the collisional dephasing of the N_2 CARS signal (resulting in the collisional Raman linewidths $\Gamma^{N_2}_{J\rightarrow J+2}$) and deduce the H_2O mole fraction according to

$$X_{H_2O} = \frac{1}{\Gamma_{J\to J+2}(N_2 - H_2O)} \left[\Gamma^{N_2}_{J\to J+2} - \sum_k X_k \cdot \Gamma_{J\to J+2}(N_2 - M_k) \right] \quad (13.7)$$

where $\Gamma_{J\to J+2}$ are the Raman linewidths due to inelastic collisions with the kth molecular perturber (N_2, O_2 or H_2) present in the probe volume with mole fraction X_k. Near collisional-independent measurements of the temperature and relative O_2/N_2 and H_2/N_2 concentrations are performed thus at short probe delay ($\tau_1 \approx 20$ ps), while the H_2O concentration is estimated by the collisional dephasing of the N_2 CARS signal at longer probe delays ($\tau_2 > 100$ ps), as shown in Fig. 13.15. The whole set of relevant scalar fields are thus measured across a laminar H_2/air diffusion flame front in [72]: temperature is measured simultaneously to all the major combustion species, yielding absolute concentration measurements of N_2, O_2, H_2, and H_2O.

As the temperature and concentrations are assumed as constant in a laminar flow, sequential measurements of the collisional dephasing of the pure-rotational N_2 CARS signal are performed, by delaying the probe pulse up to 360 ps. The extension of this diagnostic technique to turbulent flows, where the local temperature and composition fields are highly dynamic, requires the collisional dephasing to be measured simultaneously to temperature and relative O_2/N_2 and H_2/N_2 concentrations. This is achieved in [72] by employing a dual-probe CARS scheme [80–82], whereby the probe beam is split in two pulses: the first probe pulse is delayed by 20 ps with respect to the pump/Stokes pulse, the second one by 250 ps. A novel polarization approach is furthermore demonstrated in Castellanos et al., such that the two probe beams are collinear, and their linear polarization is respectively orthogonal and perpendicular to the linear polarization of the pump/Stokes beam. The resulting CARS signals are thus generated, at time $t = 20$ ps and 250 ps, with orthogonal relative polarization and can be independently recorded in the two detection channels of the polarization-sensitive coherent imaging spectrometer. Figure 13.15 shows two single-shot pure-rotational fs/ps CARS imaging spectra acquired simultaneously at 20 ps and 250 ps at the center of the turbulent canonical "H3" flame provided on the TU Darmstadt/DLR Stuttgart burner [88]. This is a turbulent jet flame, with a center fuel stream consisting of a mixture of 50% N_2–50% H_2. The first two spectral lines of H_2 are detected up to 600 cm^{-1}, allowing for simultaneous thermometry and H_2/N_2 concentration measurements in this region of the flame. The whole set of major scalar fields are thus simultaneously mapped on a single laser-shot over the 1D FOV of the fs/ps CARS instrument. An example is given in Fig. 13.16, where the temperature and absolute concentrations of O_2 and H_2O are simultaneously measured over a sample of 300 single-shot pure-rotational CARS spectra, acquired in the reaction zone of the turbulent jet flame (6.75 mm from its centerline).

The J-dependence of the collisional Raman linewidths shown in Fig. 13.17 offers an additional degree of freedom that could be exploited to extend this diagnostic approach to more complex collisional environments. For example, the time-resolved dephasing of the spectrally-integrated CARS signal could be employed to measure

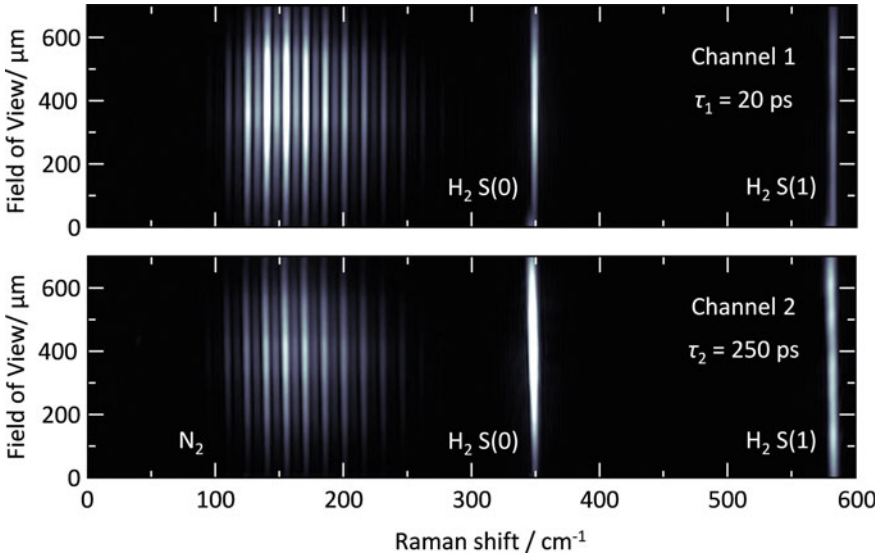

Fig. 13.15 Single-shot dual-probe fs/ps CARS imaging measurements in the turbulent canonical "H3" flame provided on the TU Darmstadt/DLR Stuttgart burner [88]. Time- and frequency-resolved hybrid fs/ps CARS allows for the simultaneous mapping of the whole set of major scalar fields in the flame: the temperature and relative O_2/N_2 and H_2/N_2 concentrations are measured in the frequency domain at $\tau_1 = 20$ ps, while the H_2O concentrations are deduced from the time-resolved collisional dephasing of the N_2 CARS signal at $\tau_2 = 250$ ps

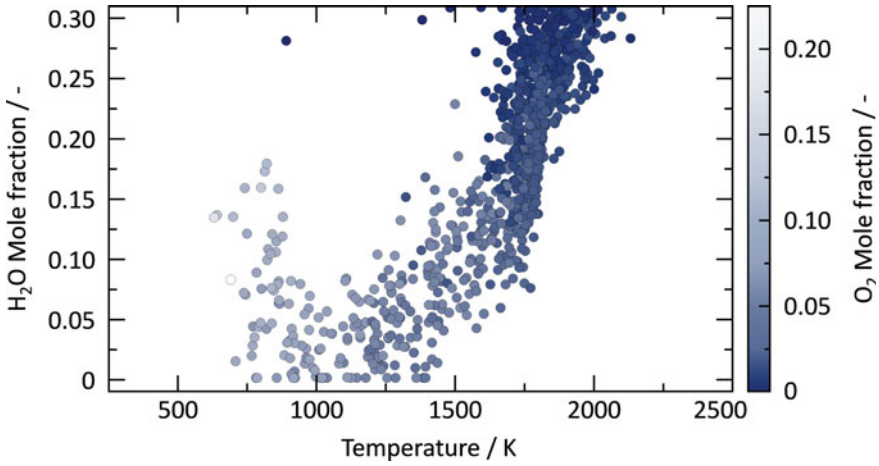

Fig. 13.16 Complete scalar characterization in a turbulent hydrogen jet flame. Each point in the scatter plot represents the local temperature and absolute O_2 and H_2O mole fractions measured 6.75 mm from the centerline of the turbulent jet flame. 300 single-shot fs/ps CARS spectra are acquired in the sample. As expected, strong positive and negative correlations are found between temperature and H_2O and O_2 mole fractions, respectively. Adapted with permission from Castellanos et al. [72]. © 2022 Elsevier Inc.

the local pressure, while the specific dephasing of well-resolved lines in the pure-rotational N_2 spectrum would be sensitive to the H_2O mole fraction. The species-specific dependence of the collisional Raman linewidths on the rotational quantum number could also allow for extending this detection scheme to another species invisible in the pure-rotational Raman spectrum, such as CH_4.

13.5 Ultrabroadband fs/ps CARS with In Situ Filamentation

Over the past ten years, the pursuit of two-beam fs/ps CARS as the ultimate laser spectroscopy for complete scalar determination in chemically reacting flows has led to the development of ultrabroadband fs/ps CARS.

This technique makes use of a compressed supercontinuum laser pulse, a single pump/Stokes pulse, to impulsively excite the pure-rotational and ro-vibrational coherence of the target molecules. Compressing the temporal duration of the pump/Stokes pulse to below ~20 fs the spectral excitation window can be extended beyond the pure-rotational region to low-frequency vibrational modes in the vibrational fingerprint region 500–1800 cm^{-1} (e.g. bending modes of hydrocarbon molecules [50, 89]). Even shorter fs laser pulses can excite the vibrations of light diatomic molecules up to the ro-vibrational Raman spectrum of H_2 at 4200 cm^{-1}, which has a vibrational period of ~8 fs [90]. Ultrabroadband fs/ps CRS can thus be used to perform simultaneous thermometry and absolute concentration measurements of all the major molecular species present in the probed volume, as well as multi-modal thermometry in non-equilibrium environments.

The first demonstration of two-beam ultrabroadband fs/ps CARS imaging for gas-phase detection was presented by Bohlin and Kliewer, who employed a hollow-core fiber and a set of chirped mirrors to generate a 7 fs compressed supercontinuum [60]. This was employed as the ultrabroadband pump/Stokes pulse in the two-beam 1D phase-matching scheme of [18] to perform wideband spectroscopy from the pure-rotational up to the C–H stretch region (~3200 cm^{-1}) of the Raman spectrum. The same authors demonstrated the full diagnostic potential of ultrabroadband fs/ps CARS imaging by achieving wideband chemical detection across a laminar premixed C_2H_4/air flame front. The simultaneous excitation of the whole Raman spectrum up to 4200 cm^{-1} and the ability of performing single-shot spatially correlated measurements across the 1D FOV allowed for the mapping across the chemical reaction layer of the flame [50]. Ultrabroadband fs/ps CARS was later employed as a combustion diagnostic tool to concurrently map the temperature and major species at the flame-wall interaction region on a side-wall-quenching burner [91]. The application of pure-rotational fs/ps CARS to perform direct thermometry on H_2 was then investigated in Courtney et al., where a 7 fs supercontinuum pump/Stokes pulse was employed to excite 8 spectral lines of the pure-rotational H_2 Raman spectrum up to ~1820 cm^{-1}.

The current state-of-the-art in ultrabroadband fs/ps CARS for gas-phase diagnostics is undoubtedly represented by the use of a compressed supercontinuum ro realize 2D hyperspectral imaging of the whole Raman spectrum up to 4200 cm^{-1} [46]. Bohlin and Kliewer demonstrated single-shot hyperspectral CARS imaging to measure the 2D temperature field over planar sections of a H_2 jet flame, as well as to simultaneously map the reactants (H_2 and O_2) distribution across the flame front.

A recent example of the use ultrabroadband fs/ps CARS for the study of industry-relevant chemical processes is found in Ran et al., where this technique was employed for the in situ investigation of carbonaceous feedstock gasification in a CO_2 atmosphere [92]. The authors employed an optical parametric chirped-pulse amplifier (OPCPA) to generate a 7 fs supercontinuum pump/Stokes pulse to simultaneously excite the ro-vibrational Raman spectra of CO_2 and CO. Simultaneous CO_2 CARS thermometry and absolute CO concentration measurements were performed in a gas oven, providing experimental insight in the carbon gasification process. The possibility of performing multiplex spectroscopy on the whole set of Raman-active species present in the probe volume, as well as accurate multi-mode thermometry, makes ultrabroadband fs/ps CARS an appealing to for a vast range of industrial applications relating to the propulsion and power generation [25, 76, 93].

Nevertheless, a number of technical difficulties need to be addressed to make ultrabroadband fs/ps CARS a mature and robust diagnostic tool for extensive use in industrial applications. The first question concerns the shot-to-shot stability of the supercontinuum light source employed to generate the ultrabroadband pump/Stokes pulse. As pointed out by Bohlin and Kliewer, the 7 fs supercontinuum output of the hollow-core fiber was affected by spectral fluctuations, which negatively

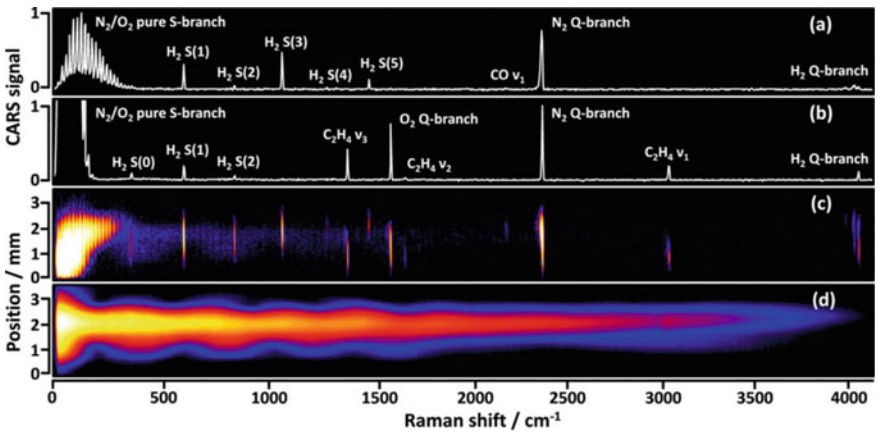

Fig. 13.17 Ultrabroadband fs/ps 1D-CARS imaging across a laminar premixed C_2H_4/air flame front. The progression of the chemical reaction along the flame front is mapped by single-shot spectral imaging along the 3 mm FOV, allowing for simultaneous thermometry and detection of all the major combustion species. Adapted with permission from Bohlin and Kliewer [50]. © 2015 American Chemical Society

affected the reproducibility of ultrabroadband fs/ps CARS thermometry resulting in a single-shot precision of ~5%, as compared to the ~1% precision of the same CARS instrument employing a 45 fs pump/Stokes pulse [50]. The main obstacle to the application of ultrabroadband fs/ps CARS in the vast majority of representative full-scale experimental platforms and industrial applications is the need to transmit the compressed supercontinuum to the measurement location. This is a non-trivial engineering problem as the large GVD introduced by the optical material of thick optical windows, in optically-accessible platforms, can reduce the effective excitation bandwidth provided by the supercontinuum pump/Stokes pulse. An example of the impact of the optical window on the effective excitation bandwidth is found in Richardson et al. where 1D pure-rotational fs/ps CARS imaging was employed to map the temperature profile in the post-detonation fireball of a commercial detonator [94]. The significant non-linear chirp introduced by the 13 mm optical window of the explosion containment housing resulted in a limitation of the excitation bandwidth to ~200 cm^{-1}. Moreover, supercontinuum fs laser pulses, having a much larger bandwidth, are even more sensitive to dispersion of their spectral components. This problem is even more significant when the harsh experimental conditions of e.g. high-pressure rocket and aircraft combustors are considered: the large vibrational, thermal and pressure loads on the optical windows can change the local GVD of the pulse to an extent that is difficult to foresee and compensate beforehand. Furthermore, even after its transmission through the optical material of the window, the supercontinuum pulse can be significantly affected by the local temperature and composition of the gas-phase medium along its path to the probe volume. As pointed out in the previous section, the unknown effective spectral excitation profile is a source of uncertainty in fs/ps CARS measurements when the ex situ referencing protocol is employed [52]. The magnitude of the GVD introduced along the optical path of the fs pump/Stokes pulse is of course larger the shorter the duration of the compressed supercontinuum pulse is. Hence, the conventional ex situ referencing protocol can be expected to introduced even larger an uncertainty to ultrabroadband fs/ps CARS measurements.

13.5.1 Soft Pulse Compression Behind Thick Optical Windows

A novel strategy for the realization of ultrabroadband fs/ps CARS measurements behind thick optical windows is introduced in Mazza et al. by employing fs laser-induced filamentation [95]. This phenomenon can be described as the non-linear propagation of high-peak irradiance fs laser pulses in transparent optical media [96]: the combination of optical Kerr effect and laser induced ionization results in cycles of self-focusing and plasma defocusing. Hence, while propagating within the resulting plasma filament, which acts a waveguide, the laser pulse experiences self-compression to a few- or even single-cycle pulse. The filamentation of fs laser pulses has been demonstrated to produce a compressed supercontinuum, which

can excite the whole set of pure-rotational and ro-vibrational Raman modes up to 4200 cm^{-1} [90, 97].

Fs laser-induced filamentation can thus be employed to achieve a "soft" pulse compression –to < 20 fs– directly behind thick optical windows, according to a strategy called "in situ generation/in situ use" of the compressed supercontinuum. In Fig. 13.18a a relatively long 35 fs pulse (1.5 mJ/pulse) is transmitted "pre-chirped" through a 22 mm-thick BK7 glass window, placed after a 500 mm spherical focusing lens, and generates a ~13 mm long filament in air. The compressed supercontinuum output by the filament acts as the ultrabroadband pump/Stokes pulse coherently exciting ro-vibrational Raman modes up to ~2000 cm^{-1} [89]. Adopting the two-beam phase-matching scheme described above, spatially-resolved measurements can be performed with the probe beam crossing the supercontinuum pump/Stokes beam 3–5 mm after the end of the filament [95].

Two remarkable observations make in situ fs laser-induced filamentation well-suited to realize ultrabroadband fs/ps CARS. On the one hand, the filament is experimentally confirmed to propagate through steep temperature and composition gradients as encountered, e.g. through the flame front of the laminar premixed CH_4/air flame in Fig. 13.18b. This is explained by the change in the effective refractive index affecting the optical Kerr effect and the plasma density to a similar extent, such that the dynamic equilibrium between self-focusing and plasma defocusing is maintained as the light propagates in this filament through the flame front. On the other hand, for increasing energy in the fs laser pulse, the optical Kerr effect determines a non-linear shift of the focus towards the focusing lens, such that the filament grows backwards and the exit position from the filament remains the same. This is crucial to guarantee the non-intrusiveness of ultrabroadband fs/ps CARS with in situ filamentation as gas-phase diagnostics tool. By maintaining the probe volume at a fixed distance

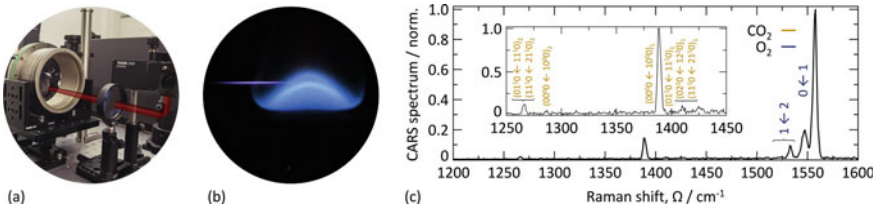

Fig. 13.18 Ultrabroadband fs/ps CARS behind thick optical windows via in situ fs laser-induced filamentation. **a** Transmission of the "pre-chirped" 35 fs pump/Stokes pulse through a 22 mm BK7 window placed ~20 cm after the 500 mm spherical focusing lens. **b** In situ generation/in situ use of the compressed supercontinuum via fs laser-induced filamentation in a laminar premixed CH_4/air flame. The CARS probe volume is located ~4 mm after the end of the filament to avoid ionization of the gas-phase medium in the probe volume and to ensure the use of this light source for non-intrusive laser diagnostics. **c** Single-shot ro-vibrational CO_2–O_2 CARS spectrum acquired in the hot products of the flame behind the optical window. At the flame temperature (T ~ 1620 K) the first vibrational hot band of in the ro-vibrational Raman spectrum of O_2 is detected, the ro-vibrational Raman spectrum of polyatomic CO_2 is much more complex and multiple hot bands are detected in the CO_2 Fermi dyad [95]

from the end of the filament, we can guarantee that no ionization is present in the probe volume [95].

The use of in situ laser-induced filamentation to perform ultrabroadband fs/ps CARS thermometry is first demonstrated in [95], by simultaneously investigating the ro-vibrational Raman spectra of O_2 and CO_2 in a laminar premixed CH_4/air flame. The performance of ro-vibrational CO_2 CARS thermometry is found to be comparable to state-of-the-art pure-rotational fs/ps CARS at temperatures higher than 2000 K. In particular, the complex ro-vibrational Raman spectrum of CO_2, consisting of the Fermi dyad shown in Fig. 13.18c, has a strong temperature dependence that makes it a suitable candidate for CARS thermometry. The precision of CO_2 CARS thermometry, assessed over a sample of 40-shot-averaged ultrabroadband CARS spectra, is better than 1% at the highest temperature measured (T ~ 2130 K). More recently, Tian and co-workers have demonstrated the use of in situ filamentation to perform single-shot ro-vibrational N_2 CARS thermometry at 1 kHz in a flat CH_4/air flame [98].

The first proof-of-principle demonstration of the in situ generation/in situ use strategy to achieve ultrabroadband fs/ps CARS behind a thick optical window is given in Mazza et al., where direct pure-rotational fs/ps CARS is employed on H_2 to measure the temperature profile across a laminar H_2/air diffusion flame [73]. As mentioned above, a 22 mm BK7 glass window is placed in the pump/Stokes beam path ~20 cm after the spherical focusing lens, such that the pulse is compressed directly behind it via in situ filamentation. The window introduces a linear chirp of 424 fs^2, as measured by attenuating the pump/Stokes to ~50 μJ/pulse to avoid the onset of filamentation and recording the NR CARS spectrum in a flow of Ar. This linear chirp is easily compensated by the external compressor unit shown in Fig. 13.5, which can pre-chirp the fs pulse introducing a linear dispersion well in excess of ±4000 fs^2. The external compressor is thus employed to control the phase of the fs pulse prior its filamentation behind the window: a negative chirp of −492 fs^2 is experimentally found to optimize the filamentation process in the H_2/air flame [73], as shown in Fig. 13.19. The resulting supercontinuum has a duration of 17 fs, as measured by the ultrabroadband NR CARS signal generated in Ar. This compressed supercontinuum has a bandwidth sufficient to impulsively excite the pure-rotational coherence of not only diatomic molecules such as O_2 and N_2, but also of H_2 whose Raman spectrum spans more than 1500 cm^{-1} at flame temperatures.

Unfortunately the ultrabroadband NR CARS spectrum in Fig. 13.19b, as recorded ex situ in a room-temperature Ar flow, is not fully representative of the ultrabroadband excitation efficiency achieved by in situ filamentation in the flame environment. As pointed out in the previous section, the NR CARS spectrum acquired ex situ cannot account for the impact of the local temperature and composition fields along the beam path to the measurement location. Furthermore, in the case of in situ generation/in situ use of the compressed supercontinuum the magnitude of the pulse self-compression via fs laser-induced filamentation strongly depends on the local temperature and composition of the gas-phase medium, as seen in Fig. 13.20. As different gases have a different electronic contribution to the third-order optical susceptibility $\chi_{NR}^{(3)}$, so

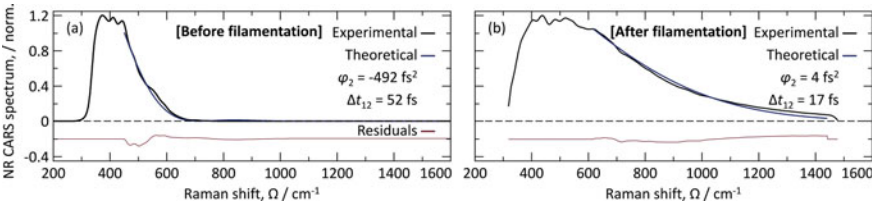

Fig. 13.19 Pump/Stokes pulse self-compression behind the optical window via in situ fs laser-induced filamentation. **a** 1000 shot-averaged NR CARS spectrum of the chirped pump/Stokes pulse, optimised for pulse compression via in situ filamentation in a laminar H_2/air diffusion flame. **b** 1000 shot-averaged ultrabroadband NR CARS spectrum generated by in situ filamentation in an Ar flow. Adapted with permission from Mazza et al. [73]. © 2022 Optica Publishing Group

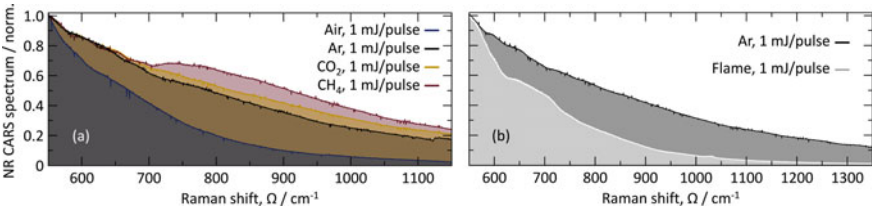

Fig. 13.20 Impact of the local boundary conditions to fs laser-induced filamentation on the in situ generation of the compressed supercontinuum. **a** Single-shot ultrabroadband NR CARS spectra generated by in situ filamentation of a 1 mJ, 35 fs TL pulse in room-temperature flows of: air (blue), Ar (black), CO_2 (yellow), and CH_4 (red). **b** Single-shot ultrabroadband NR CARS spectra generated by in situ filamentation of a 1 mJ, 35 fs TL pulse in a room-temperature flow of Ar (black) and in the hot products of a laminar H_2/air diffusion flame (gray)

does the optical Kerr effect responsible for the onset of fs laser-induced filamentation. In particular, the pulse self-compression attained by in situ filamentation in Ar is significantly larger than in air. In addition, the local temperature of the gas-phase medium has a significant impact on the non-linear refractive index of the medium, thus affecting both the magnitude of the optical Kerr effect and the plasma density inside the filament. The bandwidth of the compressed supercontinuum generated in the H_2/air flame is thus much smaller than measured ex situ in Ar: the ex situ referencing protocol is then expected to introduce a significant uncertainty in ultrabroadband fs/ps CARS with in situ filamentation.

13.5.2 Ultrabroadband fs/ps CARS with In Situ Referencing

In situ fs laser-induced filamentation is thus demonstrated to be a viable avenue to ultrabroadband fs/ps CARS behind thick optical windows. Nevertheless, the uncertainty due to the effective excitation bandwidth provided by the compressed supercontinuum pulse at the measurement location still needs to be addressed.

This is done in Mazza et al. by combining the in situ generation/in situ use of the compressed supercontinuum with the in situ referencing discussed in the previous section [73]. The polarization-sensitive coherent imaging CARS spectrometer described above is adapted to perform ultrabroadband fs/ps CARS in the vibrational fingerprint region of the Raman spectrum ~300–1500 cm^{-1}. This is done first of all by ensuring that the fs pump/Stokes pulse has linear polarization state, and that no significant ellipticity is introduced upon propagation through the optical window. A linear polarization is required to avoid the possibility of polarization ellipse rotation during the filamentation process: the compressed supercontinuum pump/Stokes pulse thus maintains the polarization of the input fs laser pulse. By choosing the appropriate relative polarization angle of the probe pulse, the ultrabroadband NR and pure-rotational H_2 CARS signals are cross-polarized. A Glan-laser polarizer (10^5 extinction ratio, Thorlabs) is employed in the polarization-sensitive spectrometer to separate the two signal components, and a broadband Fresnel rhomb rotates the linear polarization of the ultrabroadband NR CARS signal. A 100 mm imaging lens focuses the two signals onto the sCMOS detector with a dispersion of 0.93 cm^{-1}/pixel, resulting in a detection bandwidth of 1900 cm^{-1}, ultimately limited to 1200 cm^{-1} by the bandpass filter employed to suppress the co-propagating probe pulse.

The use of ultrabroadband fs/ps CARS to achieve accurate pure-rotational H2 thermometry behind the thick optical window is thus demonstrated in [73] by performing spatially resolved measurements across a laminar H_2/air diffusion flame front. The probe volume is placed ~0.5 mm above the rim of a Bunsen burner and moved at 17 radial locations from the center of the fuel stream (50% H_2–50% H_2) towards the oxidizer stream (room air). Single-shot measurements of the ultrabroadband NR and pure-rotational H_2 CARs signals are performed at each measurement location, as shown in Fig. 13.21. The NR CARS spectra acquired in situ at each location in the flame are compared to the NR CARS spectrum acquired ex situ in Ar: a dramatic change in the spectral excitation bandwidth achieved by in situ filamentation is demonstrated. The dependence of the pulse self-compression upon the local boundary conditions to the filamentation process in the flame is furthermore confirmed by the progressive reduction of the excitation bandwidth in the progression from the center of the burner towards the high-temperature reaction zone of the flame front.

Hence, the NR CARS spectrum acquired ex situ cannot faithfully map the effective excitation profile provided by the compressed supercontinuum generated via in situ filamentation in the flame. The conventional ex situ referencing protocol therefore results in a severe distortion of the normalized H_2 CARS spectra leading to a dramatic underestimation of the temperature measured by pure-rotational H_2 CARS thermometry, as shown in Fig. 13.22. Pure-rotational N_2 CARS measurements are also performed at each measurement location, providing a reference to validate the performance of pure-rotational H_2 CARS thermometry, and compare the two referencing protocols. As expected, the ex situ referencing protocol introduces a systematic bias in the measured temperature, which is larger the more the pulse compression via in situ filamentation is affected by the temperature increase in the flame. This systematic error varies from 10 to 20% at relatively low temperature in the fuel stream, up to 80% in the reaction zone of the flame. The in situ

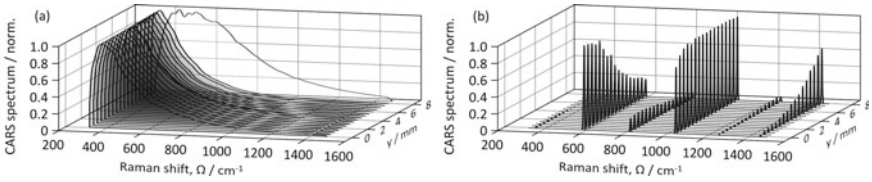

Fig. 13.21 Pure-rotational fs/ps CARS on H_2 with in situ referencing of the ultrabroadband spectral excitation. **a** 1200 shot-averaged ultrabroadband NR CARS spectra acquired in situ (black) at 17 locations from the center of the burner ($y = 0$ mm) to the flame front ($y = 8$ mm), and ex situ in room-temperature Ar (red). **b** Single-shot pure-rotational H_2 CARS spectra acquired across the flame front. Up to six pure-rotational lines are detected simultaneously over the ~300–1500 cm^{-1} spectral range. Adapted with permission from Mazza et al. [73]. © 2022 Optica Publishing Group

referencing protocol, on the contrary, allows for a correct spectral referencing of the pure-rotational H2 CARS spectra, such that the resulting accuracy is better than 1% at most measurement locations. The precision of pure-rotational H_2 CARS with in situ referencing is comparable to that of pure-rotational N_2 CARS, with a standard deviation over the 1200 single-shot spectra in each sample estimated in the range 1–3% for measurements up to location $y = 6.5$ mm. At the last three measurement locations, the reduction in the SNR due to the higher temperature and the almost complete consumption of the H_2 fuel negatively impacts the measurement precision, increasing the standard deviation up to 9% at location $y = 8$ mm.

Ultrabroadband fs/ps CARS not only allows for direct high-fidelity measurements on H_2 behind thick optical windows, but also provides new insights in the molecular transport processes taking place in the flame environment. In particular, the direct experimental observation of differential and preferential diffusion of H_2 is reported in [73]. These effects relate to the high mass diffusivity of the lightweight H_2 molecule: the former refers to its mass diffusivity coefficient being larger than other species in the combustion environment, the latter is due to the mass diffusivity being larger than the thermal diffusivity. Both effects play a critical role in the propagation of H_2 flames and their experimental quantification is critical to validate numerical modes. Differential diffusion of H_2 in the fuel stream of the laminar H_2/air diffusion flame of [73] is evident in the temperature and relative H_2/N_2 concentration profiles measured ~1 mm above the burner rim, as shown in Fig. 13.23. Within the first ~3.5 mm from the center of the burner the H_2 mole fraction reduces from 50 to 40%, while the temperature only slightly increases by ~57 K. This is due to the differential diffusion of H_2, which is transported ahead of N_2 towards the reaction zone, where is consumed in the combustion reaction.

In conclusion to the present section, it is worth noting that the in situ referencing protocol could be applied to ultrabroadband fs/ps CARS for a broader range of molecules besides H_2. The polarization approach developed for the implementation of in situ referencing protocol is applicable to any strongly depolarized Raman transition, with depolarization ratio $\rho > 0.5$. Moreover the same relative polarization angle between the pump/Stokes and probe pulses employed in the case of pure-rotational fs/ps CARS in [52, 73] (i.e. 67.8°) can be used for the in situ referencing of any

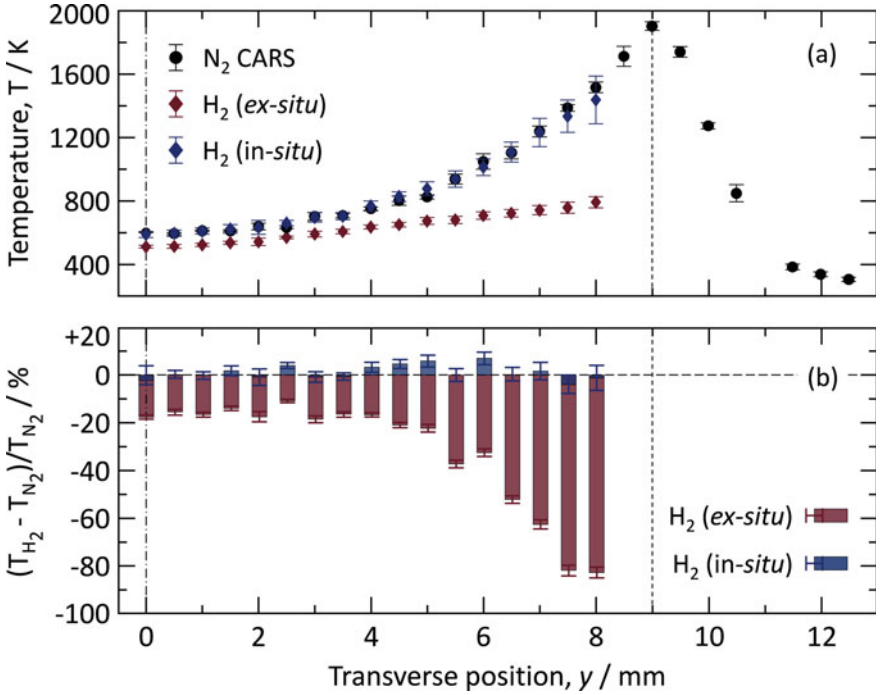

Fig. 13.22 Pure-rotational H_2 fs/ps CARS thermometry. **a** Comparison between the temperature profile across the laminar H_2/air diffusion flame front, a measured by pure-rotational N_2 and H_2 CARS thermometry. **b** Accuracy and precision of pure-rotational H_2 CARS thermometry, assuming the temperature measured by pure-rotational N_2 CARS as a reference. The conventional ex situ referencing protocol leads to a significant underestimate of the temperature measured by pure-rotational H_2 CARS. Adapted with permission from Mazza et al. [73]. © 2022 Optica Publishing Group

completely depolarized ($\rho = 0.75$) Raman spectrum. This has important implications for the possible use of ultrabroadband fs/ps CARS as a diagnostic tool for industrial chemical processes involving larger polyatomic molecules, whose least-symmetric vibrational Raman modes are often completely depolarized. An example of this is the recent use of ultrabroadband fs/ps CARS to investigate the ro-vibrational Raman spectrum associated with the ν_2 (bending) mode of CH_4 [89].

Although long-overlooked in favor of the C–H stretch (ν_1) mode, the ν_2 mode Raman spectrum offers an interesting window for the in situ monitoring of chemical and molecular transport processes in combustion environments and chemical reactors. As seen in Fig. 13.24, this Raman spectrum sits in the middle of the vibrational fingerprint region and can be simultaneously detected with other species of interest, such as O_2, CO_2 and, most importantly, H_2 [89]. The possibility of detecting CH_4 and H_2 in the same spectral window and apply the in situ referencing protocol to accurately measure their concentrations could make fs/ps CARS a powerful tool to

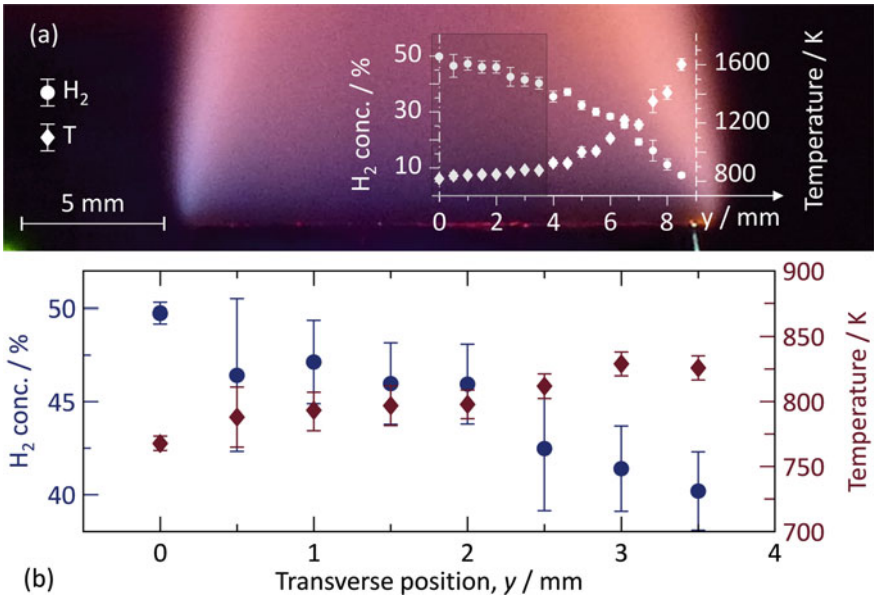

Fig. 13.23 Direct experimental observation of H_2 preferential and differential diffusion in a laminar H_2/air diffusion flame. **a** Simultaneous CARS measurement of the temperature and relative H_2/N_2 concentration across the flame front. The black box represents the area of interest for H_2 preferential diffusion. **b** While the temperature profile is almost flat in the region $y = 0$–3.5 mm the H_2 mole fraction shows a relative variation of 20%, owing to the differential diffusion of H_2 in the fuel stream. Adapted with permission from Mazza et al. [73]. © 2022 Optica Publishing Group

study the chemical reforming of CH_4 for carbon-neutral H_2 production in catalytic or plasma reactors.

13.6 Summary and Conclusions

We have illustrated some of the recent advancements in two-beam fs/ps CARS and discussed their potential towards the development of a single field-deployable diagnostic instrument for complete scalar determination in industry-relevant applications.

Two competing approaches to the extension of the two-beam fs/ps CARS instrument to simultaneous multi-fields measurements have been discussed:

- Pure-rotational fs/ps CARS imaging can achieve space-time correlated resolution, which is important for diagnostics completeness, i.e. the instrument is capable of measuring temperature, density, pressure and concentrations of major species simultaneously in gas-phase applications. In theory all the rotationally Raman-active species present in the probe volume could be detected by this technique, but in practice some of them are "invisible" in the CARS spectrum, due to their

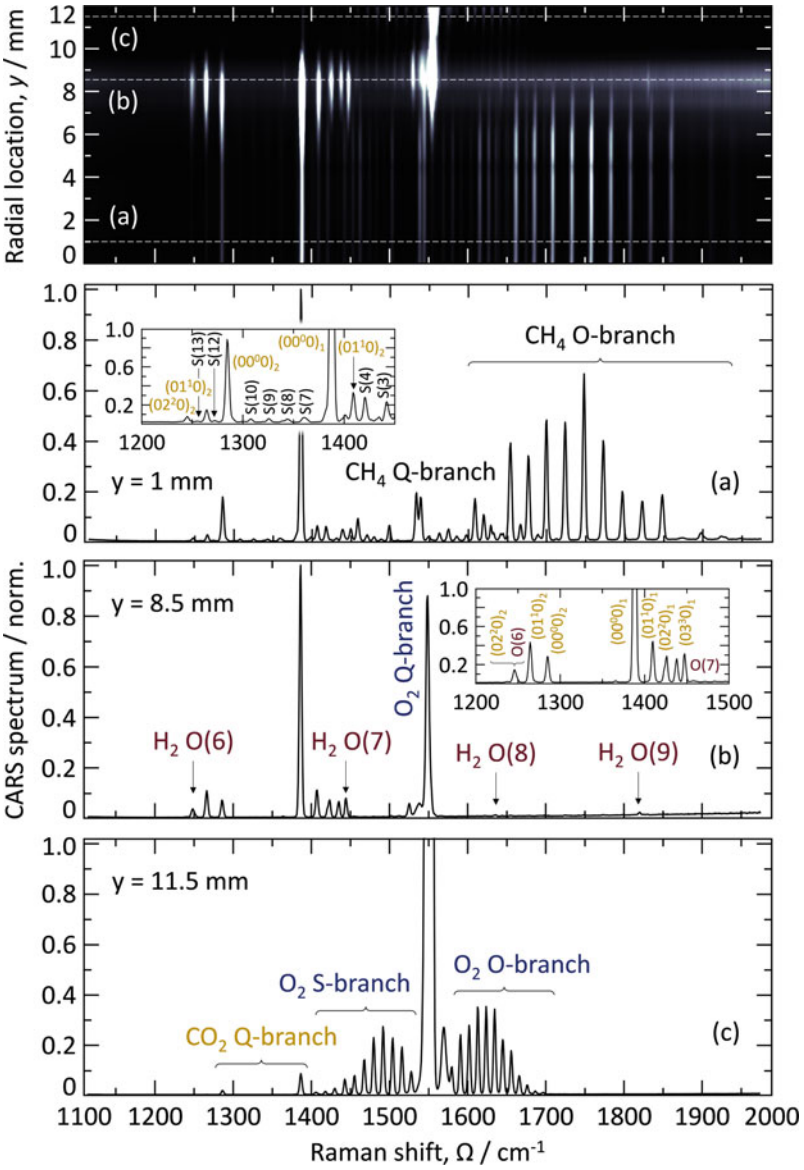

Fig. 13.24 Spatially-resolved ultrabroadband CARS in the vibrational fingerprint region of the Raman spectrum across the laminar CH_4/air diffusion flame. **a** Low-temperature ro-vibrational spectra of CO_2 and CH_4 in the fuel stream. **b** At temperatures >1300 K CH_4 pyrolysis produces H_2. Four lines of the pure-rotational H_2 CARS spectrum are detected in the spectral region ~1100–2000 cm^{-1}. **c** The oxidizer is ambient air so that the CARS spectrum is dominated by the ro-vibrational O_2 Q-branch at ~1553 cm^{-1}; a small amount of CO_2 diffuses into the oxidizer stream. Adapted with permission from Mazza et al. [89]. © 2013 AIP Publishing LLC

low rotational Raman cross-section and complex rotational structure. The use of time-resolved CARS allows for measuring concentrations of these species, via their collisional dephasing effect on the CARS signal. Furthermore, by introducing polarization control strategies for the CARS signal generation, one more "dimension" is available to CARS spectroscopy. This polarization-sensitivity can be employed to develop new diagnostic strategies for e.g. the concurrent, in situ measurements of the spectral excitation efficiency profile, or for high-sensitivity absolute concentration measurements via pure-rotational CCARS.

- Alternatively, a compressed supercontinuum pulse can simultaneously excite all the Raman-active modes to perform ultrabroadband fs/ps CARS on the pure-rotational and ro-vibrational regions of the Raman spectrum. Moreover, multi-modal CARS thermometry can be performed in non-equilibrium environments. This approach is most powerful when combined with one- or two-dimensional imaging arrangements, such that space-frequency-correlated measurements can map the in situ progression of chemical reactions and physical transport processes in rapid reacting flows. The need to transport the compressed supercontinuum through thick optical windows in industry-relevant measurement scenarios (e.g. high-pressure combustion chambers), while preserving its wide excitation bandwidth, is a long-standing limitation to the practical use of ultrabroadband fs/ps CARS. The use of fs laser-induced filamentation as an ultrabroadband coherent light source is proposed as a straightforward solution to this issue. The in situ generation/in situ use of the compressed supercontinuum is thus demonstrated to perform single-shot fs/ps CARS in the vibrational fingerprint region in laboratory flames behind a thick optical window. The impact of the local boundary conditions to the supercontinuum generation in the reacting flow is effectively quantified by the adoption of the in situ spectral referencing protocol.

Both the above-mentioned approaches can be implemented with minor modification of the same fs/ps CARS instrument, employing a single ultrafast regenerative amplifier laser system. This fs laser system design is cost-effective and greatly simplifies the operations of the CARS instrument: the need for complex beam alignment, often mentioned as a downside to CARS diagnostics, is largely relaxed with the adoption of the two-beam phase matching scheme and inherent synchronization of the two pulses. Furthermore, the introduction of an external compressor unit to pre-chirp the pump/Stokes pulses grants a large flexibility to the system in terms of its applicability in optically-accessible applications.

In conclusion, two-beam fs/ps CARS is the most-powerful diagnostic technique for high-fidelity multi-field measurements in harsh gas-phase environments and chemically reacting flows. The possibility of single-shot complete scalar determination with unparalleled spatial-temporal resolution and its robust, cost-effective implementation with a single amplified femtosecond laser system make this technique suitable for a wide range of applications with particular regard to the propulsion and power industry.

References

1. K. Kohse-Höinghaus, R.S. Barlow, M. Aldén, J. Wolfrum, Proc. Combust. Inst. **30**, 89 (2005)
2. A. Farooq, A.B.S. Alquaity, M. Raza, E.F. Nasir, S. Yao, W. Ren, Prog. Energy Combust. Sci. **91**, 100997 (2022)
3. R.L. Farrow, P.L. Mattern, L.A. Rahn, Appl. Opt. **21**, 3119 (1982)
4. A.C. Eckbreth, *Laser Diagnostics for Combustion Temperature and Species* (CRC Press, London, 1996)
5. W.R. Lempert, I.V. Adamovich, J. Phys. D Appl. Phys. **47**, 433001 (2014)
6. C.M. Penney, R.L. St. Peters, M. Lapp, J. Opt. Soc. Am. **64**, 712 (1974)
7. P.R. Régnier, J.-P.E. Taran, Appl. Phys. Lett. **23**, 240 (1973)
8. F. Moya, S.A.J. Druet, J.-P.E. Taran, Opt. Commun. **13**, 169 (1975)
9. P.D. Maker, R.W. Terhune, Phys. Rev. **137**, 801 (1965)
10. S. Roy, J.R. Gord, A.K. Patnaik, Prog. Energy Combust. Sci. **36**, 280 (2010)
11. A.C. Eckbreth, T.J. Anderson, Appl. Opt. **24**, 2731 (1985)
12. M. Aldén, P.-E. Bengtsson, H. Edner, Appl. Opt. **25**, 4493 (1986)
13. E.K. Gustafson, J.C. McDaniel, R.L. Byer, IEEE J. Quantum Electron. **QE-17**, 2258 (1981)
14. R.E. Foglesong, S.M. Green, R.P. Lucht, J.C. Dutton, AIAA J. **36**, 234 (1998)
15. A.C. Eckbreth, Combust. Flame **39**, 133 (1980)
16. F. Grisch, P. Bouchardy, W. Clauss, Aerosp. Sci. Technol. **7**, 317 (2003)
17. M. Scherman, R. Santagata, E. Lin, P. Nicolas, J.-P. Faleni, A. Vincent-Randonnier, P. Cherubini, F. Guichard, A. Mohamed, D. Gaffie, B. Attal-tretout, A. Bresson, J. Raman Spectrosc. **52**, 1643 (2021)
18. A. Bohlin, B.D. Patterson, C.J. Kliewer, J. Chem. Phys. **138**, 081102 (2013)
19. R.W. Boyd, *Nonlinear Optics*, 3rd edn. (Academic Press, 2008)
20. A.C. Eckbreth, Appl. Phys. Lett. **32**, 421 (1978)
21. D.A. Long, *The Raman Effect: a Unified Treatment of the Theory of Raman Scattering by Molecules*, 1st ed. (Wiley, 2002)
22. M. Aldén, P.-E. Bengtsson, H. Edner, S. Kröll, D. Nilsson, Appl. Opt. **28**, 3206 (1989)
23. S. Roy, T.R. Meyer, R.P. Lucht, M. Afzelius, P.-E. Bengtsson, J.R. Gord, Opt. Lett. **29**, 1843 (2004)
24. C. Brackmann, J. Bood, M. Afzelius, P.-E. Bengtsson, Meas. Sci. Technol. **15**, 13 (2004)
25. T.R. Meyer, S. Roy, R.P. Lucht, J.R. Gord, Combust. Flame **142**, 52 (2005)
26. R.J. Hall, Combust. Flame **35**, 47 (1979)
27. I.R. Beattie, T.R. Gilson, D.A. Greenhalgh, Nature **276**, 378 (1978)
28. A. Bohlin, F. Vestin, P. Joubert, P.-E. Bengtsson, J. Raman Spectrosc. **40**, 788 (2009)
29. S. Kröll, M. Aldén, T. Berglind, R.J. Hall, Appl. Opt. **26**, 1068 (1987)
30. R.P. Lucht, P.J. Kinnius, S. Roy, J.R. Gord, J. Chem. Phys. **127**, 044316 (2007)
31. J.D. Miller, C.E. Dedic, S. Roy, J.R. Gord, T.R. Meyer, Opt. Express **20**, 5003 (2012)
32. M. Afzelius, P.-E. Bengtsson, J. Bood, J. Bonamy, F. Chaussard, H. Berger, T. Dreier, Appl. Phys. B **75**, 771 (2002)
33. C.J. Kliewer, A. Bohlin, E. Nordström, B.D. Patterson, P.E. Bengtsson, T.B. Settersten, Appl. Phys. B **108**, 419 (2012)
34. C. Meißner, J.I. Hölzer, T. Seeger, Appl. Opt. **58**, 47 (2019)
35. W.D. Kulatilaka, H.U. Stauffer, J.R. Gord, S. Roy, Opt. Lett. **36**, 4182 (2011)
36. C.J. Kliewer, Opt. Lett. **37**, 229 (2012)
37. A. Bohlin, C.J. Kliewer, J. Chem. Phys. **138**, 221101 (2013)
38. B.D. Prince, A. Chakraborty, B.M. Prince, H.U. Stauffer, J. Chem. Phys. **125**, 044502 (2006)
39. S. Legros, C. Brunet, P. Domingo-Alvarez, P. Malbois, E. Salaun, G. Godard, M. Caceres, B. Barviau, G. Cabot, B. Renou, G. Lartigue, V. Moureau, S. Puggelli, S. Richard, M. Abdelkrim, F. Grisch, Combust. Flame **224**, 273 (2021)
40. C.E. Dedic, T.R. Meyer, J.B. Michael, Optica **4**, 563 (2017)
41. S.A. Steinmetz, T.Y. Chen, B.M. Goldberg, C.M. Limbach, C.J. Kliewer, Opt. Lett. **47**, 5429 (2022)

42. S. Roy, P. Wrzesinski, D. Pestov, T. Gunaratne, M. Dantus, J.R. Gord, Appl. Phys. Lett. **95**, 074102 (2009)
43. A. Bohlin, M. Mann, B.D. Patterson, A. Dreizler, C.J. Kliewer, Proc. Combust. Inst. **35**, 3723 (2015)
44. D. Escofet-Martin, A.O. Ojo, N.T. Mecker, M.A. Linne, B. Peterson, Proc. Combust. Inst. **38**, 1579 (2021)
45. A. Bohlin, C.J. Kliewer, J. Phys. Chem. Lett. **5**, 1243 (2014)
46. A. Bohlin, C.J. Kliewer, Appl. Phys. Lett. **105**, 161111 (2014)
47. L. Castellanos, F. Mazza, D. Kliukin, A. Bohlin, Opt. Lett. **45**, 4662 (2020)
48. S.P. Kearney, D.J. Scoglietti, Opt. Lett. **38**, 833 (2013)
49. T.L. Courtney, N.T. Mecker, B.D. Patterson, M. Linne, C.J. Kliewer, Appl. Phys. Lett. **114**, 101107 (2019)
50. A. Bohlin, C.J. Kliewer, J. Phys. Chem. Lett. **6**, 643 (2015)
51. J. Barros, M. Scherman, E. Lin, N. Fdida, R. Santagata, B. Attal-Tretout, A. Bresson, Opt. Express **28**, 34656 (2020)
52. F. Mazza, L. Castellanos, D. Kliukin, A. Bohlin, Proc. Combust. Inst. **38**, 1895 (2021)
53. S.M. Correa, Combust. Sci. Technol. **87**, 329 (1993)
54. S.P. Kearney, Combust. Flame **162**, 1748 (2015)
55. D.R. Richardson, H.U. Stauffer, S. Roy, J.R. Gord, Appl. Opt. **56**, 37 (2017)
56. Z. Tian, H. Zhao, H. Wei, Y. Tan, Y. Li, Appl. Opt. **61**, 4500 (2022)
57. M. Pealat, P. Bouchardy, M. Lefebvre, J.-P.E. Taran, Appl. Opt. **24**, 1012 (1985)
58. E.H. van Veen, D.J.E.M. Roekaerts, Appl. Opt. **44**, 6995 (2005)
59. D.K. Lauriola, P.S. Hsu, N. Jiang, M.N. Slipchenko, T.R. Meyer, S. Roy, Opt. Lett. **46**, 5489 (2021)
60. A. Bohlin, C.J. Kliewer, Appl. Phys. Lett. **104**, 031107 (2014)
61. J.E. Retter, D.R. Richardson, S.P. Kearney, Appl. Phys. B **126**, 1 (2020)
62. R.P. Lucht, R.E. Palmer, M.A. Maris, Opt. Lett. **12**, 386 (1987)
63. E. Nordström, A. Bohlin, P.-E. Bengtsson, J. Raman Spectrosc. **44**, 1322 (2013)
64. C. Brackmann, J. Bood, P.-E. Bengtsson, T. Seeger, M. Schenk, A. Leipertz, Appl. Opt. **41**, 564 (2002)
65. R.J. Hall, J.A. Shirley, A.C. Eckbreth, Opt. Lett. **4**, 87 (1979)
66. R.J. Hall, J.A. Shirley, Appl. Opt. **37**, 196 (1983)
67. D.A. Greenhalgh, R.J. Hall, F.M. Porter, W.A. England, J. Raman Spectrosc. **15**, 71 (1984)
68. F.M. Porter, D.R. Williams, Appl. Phys. B **54**, 103 (1992)
69. G. Herzberg, *Molecular Spectra and Molecular Structure. I. Spectra of Diatomic Molecules*, 2nd edn. (Van Nostrand Reinhold Company, Inc., 1950)
70. T.L. Courtney, A. Bohlin, B.D. Patterson, C.J. Kliewer, J. Chem. Phys. **146**, 224202 (2017)
71. J.E. Retter, G.S. Elliott, Appl. Opt. **58**, 2557 (2019)
72. L. Castellanos, F. Mazza, A. Bohlin, Proc. Combust. Inst. **39**, 1279 (2022)
73. F. Mazza, A. Stutvoet, L. Castellanos, D. Kliukin, A. Bohlin, Opt. Express **30**, 35232 (2022)
74. A. Montello, Z. Yin, D. Burnette, I.V. Adamovich, W.R. Lempert, J. Phys. D Appl. Phys. **46**, 464002 (2013)
75. J. Zhu, A. Ehn, J. Gao, C. Kong, M. Aldén, M. Salewski, F. Leipold, Y. Kusano, Z. Li, Opt. Express **25**, 20243 (2017)
76. S.A. Tedder, J.L. Wheeler, A.D. Cutler, P.M. Danehy, Appl. Opt. **49**, 1305 (2010)
77. F. Vestin, M. Afzelius, P.-E. Bengtsson, Proc. Combust. Inst. **31**, 833 (2007)
78. D. Kliukin, A. Bohlin, Patent P126758NL00/*Simultaneous Space-Time Resolution Broadband Coherent Raman Microscope with In-Situ Spectral Referencing* (2021)
79. D. Kliukin, F. Mazza, L. Castellanos, A. Bohlin, J. Raman Spectrosc. **52**, 1589 (2021)
80. B.D. Patterson, Y. Gao, T. Seeger, C.J. Kliewer, Opt. Lett. **38**, 4566 (2013)
81. S.P. Kearney, P.M. Danehy, Opt. Lett. **40**, 4082 (2015)
82. D. Escofet-Martin, A.O. Ojo, J. Collins, N.T. Mecker, M.A. Linne, B. Peterson, Opt. Lett. **45**, 4758 (2020)
83. L. Gong, W. Zheng, Y. Ma, Z. Huang, Nat. Photonics **14**, 115 (2020)

84. Z. Liu, J. Yao, H. Zhang, B. Xu, J. Chen, F. Zhang, Z. Zhang, Y. Wan, W. Chu, Z. Wang, Y. Cheng, Phys. Rev. A **101**, 043404 (2020)
85. J. Jiang, X. Jiang, M. Zhu, Int. J. Hydrog. Energy **40**, 15709 (2015)
86. N. Owschimikow, F. Königsmann, J. Maurer, P. Giese, A. Ott, B. Schmidt, N. Schwentner, J. Chem. Phys. **133**, 044311 (2010)
87. J. Bonamy, D. Robert, J.M. Hartmann, M.L. Gonze, R. Saint-Loup, H. Berger, J. Chem. Phys. **91**, 5916 (1989)
88. W. Meier, S. Prucker, M.-H. Cao, W. Stricker, Combust. Sci. Technol. **118**, 293 (1996)
89. F. Mazza, O. Thornquist, L. Castellanos, T. Butterworth, C. Richard, V. Boudon, A. Bohlin, J. Chem. Phys. **158**, 094201 (2023)
90. J.H. Odhner, D.A. Romanov, R.J. Levis, Phys. Rev. Lett. **103**, 075005 (2009)
91. A. Bohlin, C. Jainski, B.D. Patterson, A. Dreizler, C.J. Kliewer, Proc. Combust. Inst. **36**, 4557 (2017)
92. Y. Ran, A. Boden, F. Küster, F. An, A. Richter, S. Guhl, S. Nolte, R. Ackermann, Appl. Phys. Lett. **119**, 243905 (2021)
93. A.D. Cutler, L.M.L. Cantu, E.C.A. Gallo, R. Baurle, P.M. Danehy, R. Rockwell, C. Goyne, J. McDaniel, AIAA J. **53**, 2762 (2015)
94. D.R. Richardson, S.P. Kearney, D.R. Guildenbecher, Proc. Combust. Inst. **38**, 1657 (2021)
95. F. Mazza, N. Griffioen, L. Castellanos, D. Kliukin, A. Bohlin, Combust. Flame **237**, 111738 (2022)
96. A. Couairon, A. Mysyrowicz, Phys. Rep. **441**, 47 (2007)
97. F. Calegari, C. Vozzi, S. De Silvestri, S. Stagira, Opt. Lett. **33**, 2922 (2008)
98. Z. Tian, H. Zhao, Y. Gao, H. Wei, Y. Tan, Y. Li, Appl. Phys. Lett. **121**, 081102 (2022)